Cell Reports

Resource

Active maintenance of CD8$^+$ T cell naivety through regulation of global genome architecture

Graphical abstract

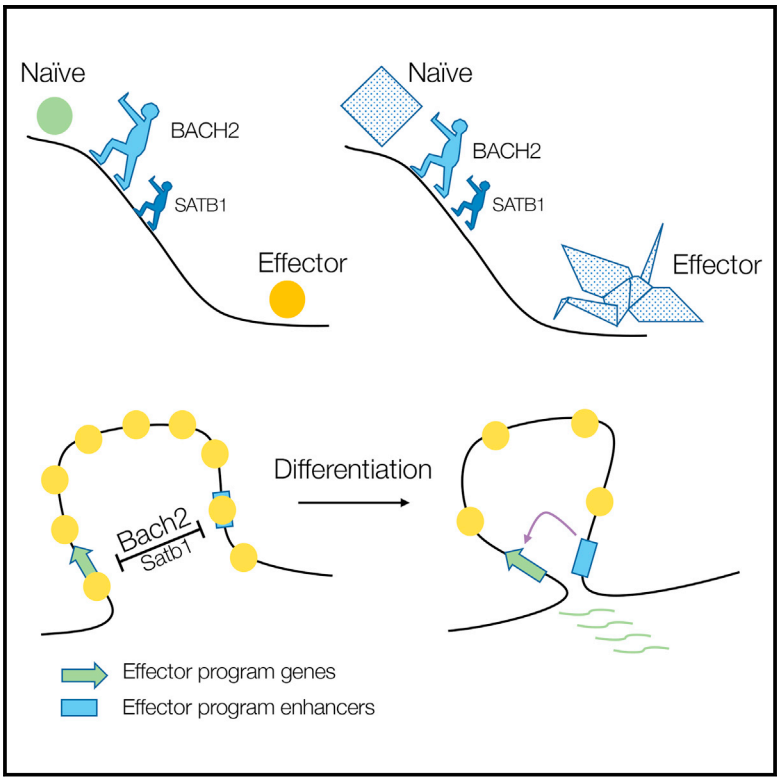

Authors

Brendan E. Russ, Adele Barugahare, Pushkar Dakle, ..., David Powell, Ananda W. Goldrath, Stephen J. Turner

Correspondence

brendan.russ@monash.edu (B.E.R.), stephen.j.turner@monash.edu (S.J.T.)

In brief

Russ et al. use Hi-C to map chromatin architecture dynamics during virus-specific CD8$^+$ T cell differentiation. They demonstrate that key transcription factors preserve naivety by enforcing a naive chromatin state, and that effector and memory states are largely similar, providing a molecular explanation for rapid memory T cell function.

Highlights

- CD8$^+$ T cell differentiation states are underscored by distinct chromatin looping architectures
- Chromatin loops connect CD8$^+$ T cell subset-specific enhancers, transcription factors and genes
- Effector and memory CTLs have similar genome architectures, explaining rapid memory recall
- BACH2, and to a lesser extent, SATB1, enforce a naive CD8$^+$ T cell loop architecture

Russ et al., 2023, Cell Reports *42*, 113301
October 31, 2023
https://doi.org/10.1016/j.celrep.2023.113301

CellPress

Cell Reports

CellPress
OPEN ACCESS

Resource

Active maintenance of CD8+ T cell naivety through regulation of global genome architecture

Brendan E. Russ,[1,*] Adele Barugahare,[1,2] Pushkar Dakle,[1] Kirril Tsyganov,[1,2] Sara Quon,[3] Bingfei Yu,[3] Jasmine Li,[1,4] Jason K.C. Lee,[1] Moshe Olshansky,[1] Zhaohren He,[4] Paul F. Harrison,[2] Michael See,[2] Simone Nussing,[5] Alison E. Morey,[1] Vibha A. Udupa,[1] Taylah J. Bennett,[1] Axel Kallies,[6] Cornelis Murre,[4] Phillipe Collas,[7,8] David Powell,[2] Ananda W. Goldrath,[3] and Stephen J. Turner[1,9,*]

[1]Department of Microbiology, Immunity Theme, Biomedical Discovery Institute, Monash University, Clayton, VIC, Australia
[2]Bioinformatics Platform, Biomedical Discovery Institute, Monash University, Clayton, VIC, Australia
[3]Department of Biological Sciences, University of California, San Diego, San Diego, CA, USA
[4]Department of Molecular Biology, University of California, San Diego, San Diego, CA, USA
[5]Peter MacCallum Cancer Centre, Melbourne, VIC, Australia
[6]Department of Microbiology and Immunology, The Peter Doherty Institute for Infection and Immunity, The University of Melbourne, Melbourne, VIC, Australia
[7]Department of Molecular Medicine, Institute of Basic Medical Sciences, University of Oslo, Oslo, Norway
[8]Department of Immunology and Transfusion Medicine, Oslo University Hospital, Oslo, Norway
[9]Lead contact
*Correspondence: brendan.russ@monash.edu (B.E.R.), stephen.j.turner@monash.edu (S.J.T.)
https://doi.org/10.1016/j.celrep.2023.113301

SUMMARY

The differentiation of naive CD8+ T lymphocytes into cytotoxic effector and memory CTL results in large-scale changes in transcriptional and phenotypic profiles. Little is known about how large-scale changes in genome organization underpin these transcriptional programs. We use Hi-C to map changes in the spatial organization of long-range genome contacts within naive, effector, and memory virus-specific CD8+ T cells. We observe that the architecture of the naive CD8+ T cell genome is distinct from effector and memory genome configurations, with extensive changes within discrete functional chromatin domains associated with effector/memory differentiation. Deletion of BACH2, or to a lesser extent, reducing SATB1 DNA binding, within naive CD8+ T cells results in a chromatin architecture more reminiscent of effector/memory states. This suggests that key transcription factors within naive CD8+ T cells act to restrain T cell differentiation by actively enforcing a unique naive chromatin state.

INTRODUCTION

Activation of naive CD8+ T lymphocytes triggers a program of clonal expansion and differentiation, resulting in a large pool of effector cytotoxic T cells (CTL) that acquire a variety of lineage-specific effector functions that enable killing of virus-infected cells and tumors. This acquired functional capacity includes the expression of cytotoxic molecules (granzymes A, B, and K, and perforin)[1] and pro-inflammatory chemokines and cytokines such as CCL4 (MIP1α), CCL5 (RANTES),[2,3] interferon-gamma (IFNγ) and tumor necrosis factor.[4] Upon resolution of infection, a long-lived pool of virus-specific (memory) CTLs is established that, relative to naive T cells, elicit effector functions rapidly following re-infection without the need for further differentiation, thus providing the basis of T cell-mediated immunity to subsequent infection.[5–7] While it is well established that the different phenotypes and functional capacities of naive, effector, and memory T cells are underscored by unique transcriptomes,[5,8] how these transcriptional profiles arise and are maintained is not fully understood.

Within eukaryotic cells, DNA is associated with histone protein complexes (nucleosomes) forming chromatin.[9] Changes to the structure of chromatin result in coordinated changes in gene transcription that underly the processes of cellular differentiation, including lineage commitment and acquisition of lineage identity within developing and mature immune cells.[8,10–13] Transcriptional enhancers act as targets for transcription factor (TF) binding that can directly and indirectly activate or repress gene transcription.[3,8,13,14] For instance, TFs including TBET,[15] BLIMP1,[16,17] and IRF4,[18] drive acquisition of effector function within CD8+ T cells, while TCF1[19] and FOXO1[20,21] are required to maintain the quiescence and stemness of naive T cells. Importantly, transcriptional networks that drive alternate differentiation states act in opposition to enable maintenance of cellular identity. For instance, FOXO1 contributes to CD8+ T cell naivety by driving expression of BACH2.[20] BACH2, in-turn, limits effector CTL differentiation by occupying enhancers and promoters of CTL effector lineage determining genes that would otherwise be bound by the AP-1 family of TFs. This effectively inhibits transcriptional activation of genes such as *Prdm1* (which encodes BLIMP1) that drive the effector transcriptional program.[22]

Enhancers can occur kilobases to megabases from the genes that they regulate, conveying their effects on gene transcription via chromatin looping that brings enhancers and their target gene promoters into close proximity.[23,24] This interaction likely allows regulatory modules (TFs and chromatin-modifying proteins) assembled at the enhancer to interact with the target promoter. For instance, TBET binds to several enhancers at the *Ifng* locus in CD4$^+$ T cells and CTLs, where it drives induction of *Ifng* transcription following activation.[15] TBET also recruits CCCTC-binding factor (CTCF), which mediates loop formation, including at the *Ifng* locus.[25] TF-dependent chromatin structuring that enables enhancer:promoter interactions has been shown to control acquisition of other lineage-specific genes in T cells, including *Il2*,[26] and *Il4/Il5/Il13*.[27–29] More recently, it was demonstrated that TCF-1 and LEF-1 are critical for ensuring naive CD8$^+$ T cell identity by maintaining a 3-dimensional genome organization that represses expression of non-CD8$^+$ T cell lineage genes.[30] Hence, lineage fidelity is maintained at the level of chromatin architecture, and localized chromatin restructuring coincides with T cell differentiation and acquisition of lineage-specific function. However, the extent to which reorganization of *cis*-regulatory elements modulates CD8$^+$ T cell differentiation remains unknown. Here, we aimed to address this question by mapping genome-wide *cis*-regulatory interactions to determine how these underpin functional and phenotypic characteristics during virus-specific CTL differentiation.

RESULTS

Mapping changes in genome architecture at distinct stages of virus-specific CTL differentiation

We and others have reported that CD8$^+$ T cell differentiation is associated with changes in histone biochemical modifications, and chromatin accessibility.[3,8,11,12,31,32] However, these data do not provide information about changes in the spatial organization of chromatin, particularly those involving non-coding regulatory elements. To determine if acquisition and maintenance of CTL lineage function following virus infection is linked to changes in global chromatin architecture, we performed *in situ* Hi-C,[33] using adoptive transfer of naive (CD44^{lo}CD62L^{hi}) OT-I TCR transgenic CD8$^+$ T cells (CD45.1$^+$) specific for the ovalbumin peptide ($OVA_{257-264}$), followed by intranasal (i.n.) infection with the influenza A/HKx31-OVA virus.[34] Virus-specific CTLs were isolated at effector (d10) and memory (>d60) time points post infection (p.i.) for comparison with naive OT-1s. Further, data from CD4$^+$CD8$^+$ (double-positive; DP) thymocytes was captured to enable an ontogenically defined context for comparison of our virus-specific CTL datasets. In total we mapped 2.17 billion contacts across the four cell states, corresponding to a total of 55,960 unique chromatin loops (Table S1).

We initially assessed gross genome organization by calculating eigenvectors at 1Mb resolution and allocating regions into either A or B genomic compartments, which broadly reflect the spatial separation of active and repressed chromatin regions, respectively.[33] To validate our compartment assignments, we overlaid ATAC-seq performed on matching samples (Figure S1A), finding that chromatin accessibility was enriched within regions of the genome assigned to the A compartment in naive, effector, and memory CD8$^+$ T cells, as expected (Figures S1B and S1C). Further, a similar relationship was found for histone modifications that identify enhancers and gene promoters (H3K4me2 and H3K4me3, respectively), while the repressive H3K27me3 modification was more evenly distributed across the A and B compartments (Figure S1B). While gross changes in compartmentalization were not observed between differentiation states (Figure S1D), some small-scale transitions were identified (Figure 1A). For example, 290 genes moved from an A to B compartment and 773 genes moved from B to A compartments upon naive to effector CD8$^+$ T cell differentiation. However, these changes in compartmentalization were not associated with changes in gene transcription (Figure 1B). Thus, movement of genes between compartments is not a significant means by which CTL differentiation is regulated following virus infection.

Topological associated domains (TADs) are large-scale genomic structures that have been reported to be largely invariant across cell types and species.[35–38] However, more recently, it was reported that the precise position of TAD boundaries is regulated to orchestrate transcriptional changes that underscore T cell development.[39] To examine TAD structures and dynamics during CD8$^+$ T cell differentiation, we identified TADs at 50 kb resolution[40] (see STAR methods), finding that the number (2,937 – DP, 2,873 – naive, 2,715 – effector, 2,923 – memory) and mean size of TADs was similar between differentiation states (Figures 1C and 1D). While TAD numbers did not vary significantly between differentiation states, we found that the precise positioning of TAD boundaries was variable, with only ~25% of TADs precisely sharing boundaries between naive and effector cells (Figure 1E), although this overlap increased to ~60% if boundaries were extended by 150 kb, indicating that the shift in TAD position was relatively small. Interestingly, and suggesting increased similarity between effector and memory genome architectures, effector and memory T cells had more common TAD boundaries than either state did with naive (Figure S1E).

While TAD boundaries were variable between differentiation states, analysis of intra-TAD interaction frequencies suggested that regulation of chromatin interactions within TADs was a key differentiator among naive, effector, and memory CD8$^+$ T cell states (Figure 1F). Hence, there appeared to be a significant remodeling of chromatin architecture with CD8$^+$ T cell differentiation, particularly at a more localized scale.

CD8$^+$ T cell differentiation is associated with intra-TAD reorganization

A multidimensional scaling analysis (MDS) was performed comparing *cis* interaction frequencies within 50 kb bins between samples (Figure 2A). We found a close grouping of biological replicates, with DP thymocytes sitting in a different space group compared with naive CD8$^+$ T cells, and naive CD8$^+$ T cells clustering separately from effector and memory states in PC1. Interestingly, effector and memory CD8$^+$ T cells clustered closely to one another in this dimension, suggesting that they shared a similar chromatin architecture. To identify genomic regions underscoring the separation of samples identified in our MDS analysis, we generated heatmaps of the Hi-C data that identified regions with varying interaction frequencies (IFs) among naive, effector, and memory CD8$^+$ T cell differentiation states, and

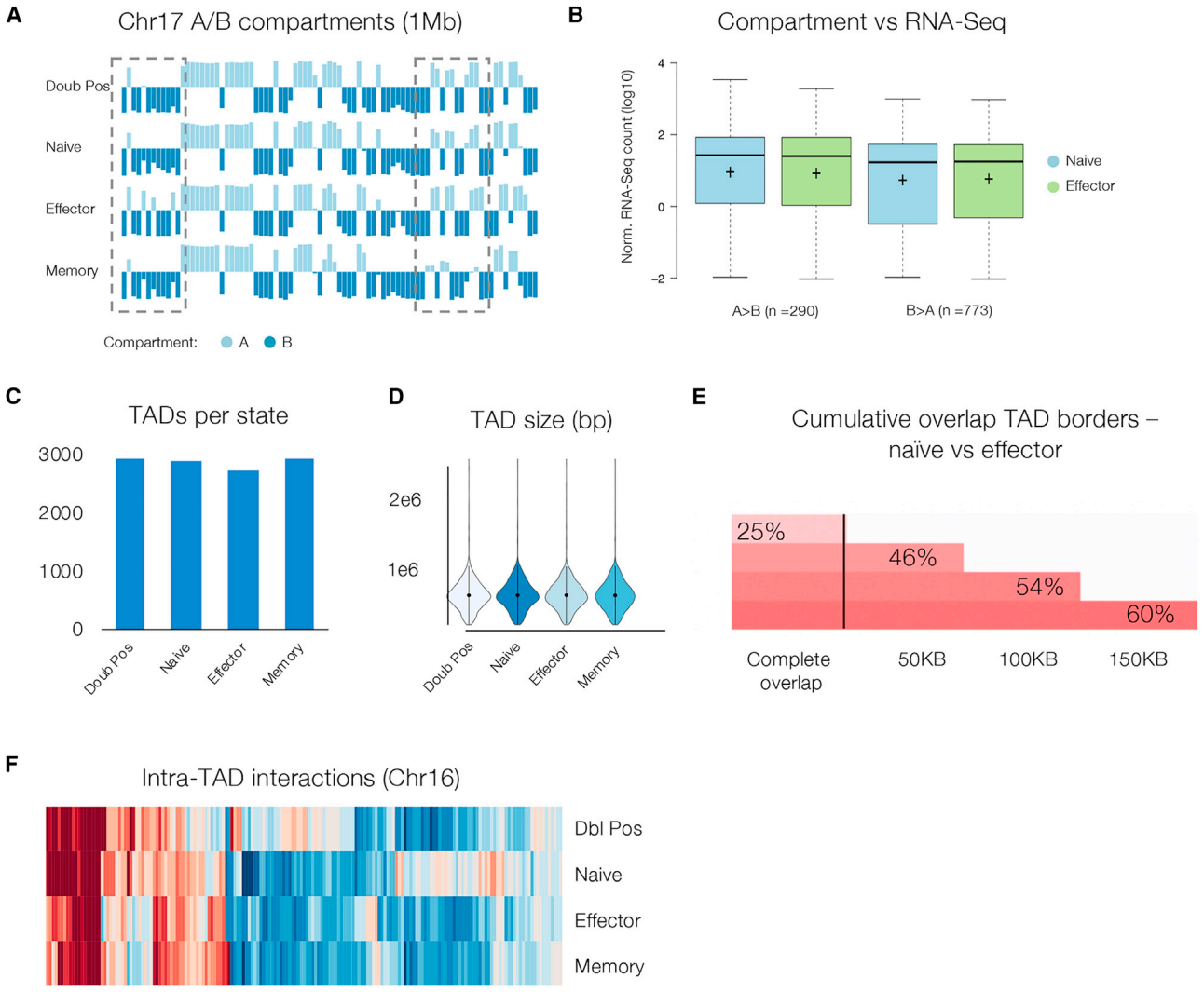

Figure 1. Analysis of higher-order chromatin structures during CTL differentiation

Sort purified, naive ($CD44^{lo}CD62L^{hi}$) $CD45.1^{+}$ $CD8^{+}$ OT-I CTLs were adoptively transferred into $CD45.2^{+}$ congenic C57BL/6J mice prior to recipients being infected with A/HKx31-OVA. Effector ($CD44^{hi}$ $CD62L^{lo}$) and memory ($CD44^{hi}$) OT-Is were isolated and sort purified either 10 or 60 days p.i., respectively, and then subjected to Hi-C. Virus-specific $CD8^{+}$ T cells were compared with sort purified $CD4^{+}CD8^{+}$ (double-positive) thymocytes from C57BL/6J mice.

(A) Eigenvectors calculated at 1Mb resolution for chromosome 17 of naive CTL, with A and B compartments shown in light blue and dark blue, respectively. Minor changes in A/B compartment structure was observed between differentiation states (dashed boxes), compartment structures and proportion of the genome in each compartment was largely conserved with differentiation.

(B) Changes in compartment from A to B and B to A with differentiation did not, on average, coincide with changes in gene transcription. Changes in A/B compartment upon naive (blue) to effector (green) differentiation versus average transcript frequency (log counts per million [cpm]) are shown as an example. (C and D) The number and average size of TADs for each differentiation state.

(E) The frequency of shared TAD borders between naive and effector Hi-C data determined at 50 kb, 100 kb, and 150 kb bin sizes (F) Heatmaps showing interaction frequency within 50 Mb windows of chr16, for DP, naive, effector, and memory CTL.

overlaid this with matched ATAC-seq data to measure changes in chromatin accessibility (Figures 2B–2F). Further, large-scale differences in IFs (referred to as Domains) were identified by calculating pairwise correlations between each differentiation state using 50-kb bins (Figures 2B–2F). While we found that most bins showed strongly correlated IFs between states, we identified a number of domains that exhibited structural changes visible as large-scale loss (Figures 2B–2D) and gain (Figures 2E and 2F) of IF. Importantly, these changes in contact frequency were also associated with changes in chromatin accessibility and gene transcription (Figures 2G–2K). For instance, loss of IF at loci encoding *Sox4*, *Prickle1,* and *Satb1* occurred upon differentiation of naive $CD8^{+}$ T cells to effector and memory states, and was associated with loss of chromatin accessibility and gene transcription (Figures 2B–2D), while gain of IF at loci such as *Prdm1* (encoding BLIMP1) and *Dmrta1* was associated with increased chromatin accessibility and gene transcription (Figures 2E and 2F). Other genes occurring within regions that

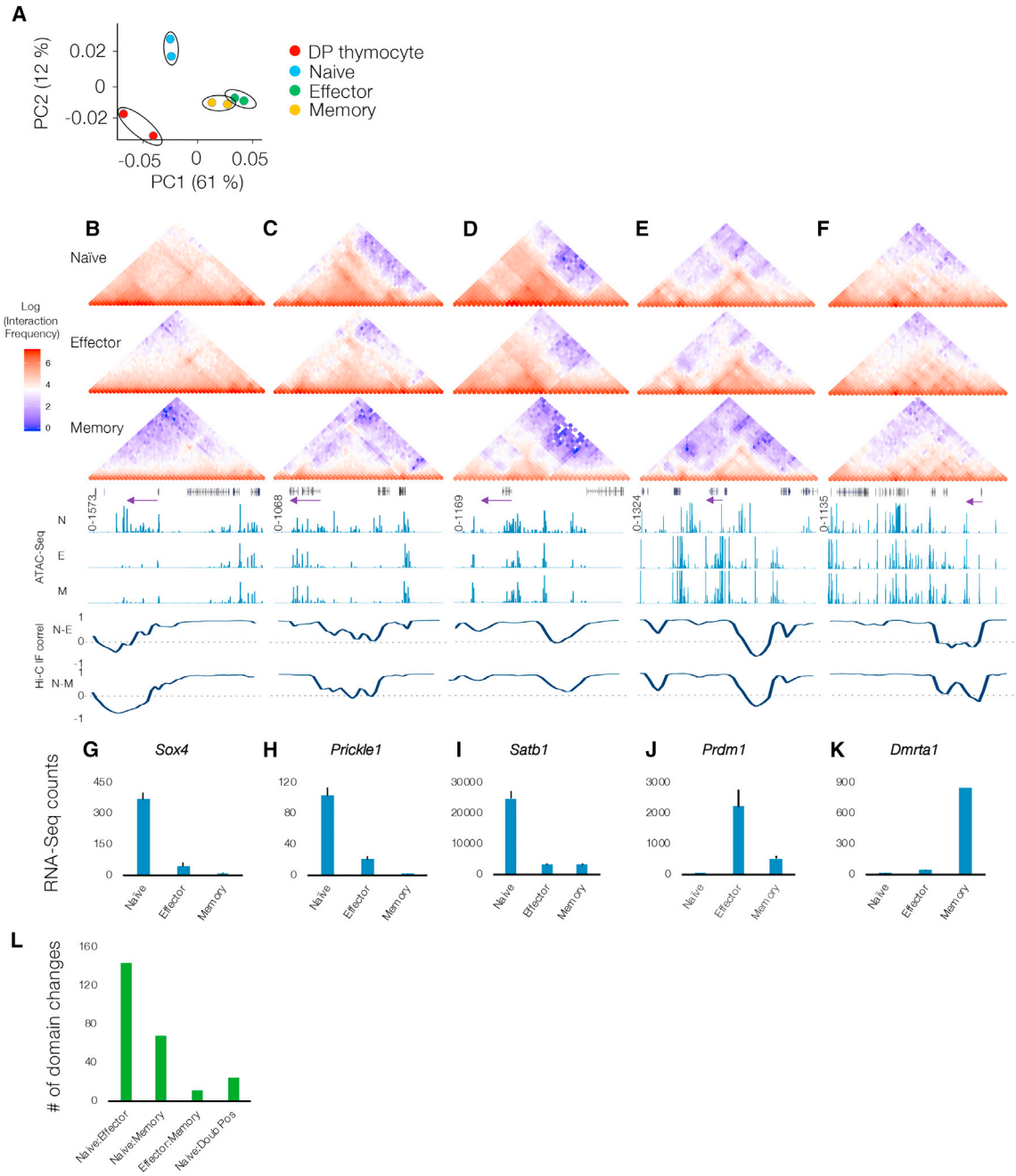

Figure 2. Distinct higher-order chromatin structures within distinct CD8⁺ T cell populations

(A) MDS plot showing relationship between Hi-C samples derived from double-positive ($CD4^+CD8^+$) thymocytes, naive, effector, and memory OT-1 $CD8^+$ T cells.

(B–F) Hi-C data (50 kb bins) normalized using ICED method showing interaction frequency at *Sox4*, *Prickle1*, *Satb1*. *Prdm1,* and *Drmta1* loci, respectively, in naive, effector, and memory OT-1 $CD8^+$ T cells. Tracks below memory panels show gene structures, with purple arrow highlighting genes of interest and their direction of transcription. Locus coordinates for (B)–(F) are: *Sox4* chr13: 28,125,000–30,325,000; *Prickle1* chr15: 93,000,000–95,000,000; *Satb1* chr17: 51,200,000–53,000,000,. *Prdm1* chr10: 43,500,000–45,500,000, and *Dmrta1* chr4:88,000,000–90,000,000. Shown below gene tracks are ATAC-seq normalized read counts for each locus in the naive, effector, and memory states Hi-C correlations are shown as pairwise comparisons of binned interaction frequencies (50 kb) for naive and effector (N-E), and naive and memory (N–M) samples, with dotted line indicating 0 on the y axis.

(G–K) Normalized RNA-seq counts[8] for each gene loci listed.

(L) Quantification of domain changes identified by pairwise correlation (50 kb) analysis depicted.

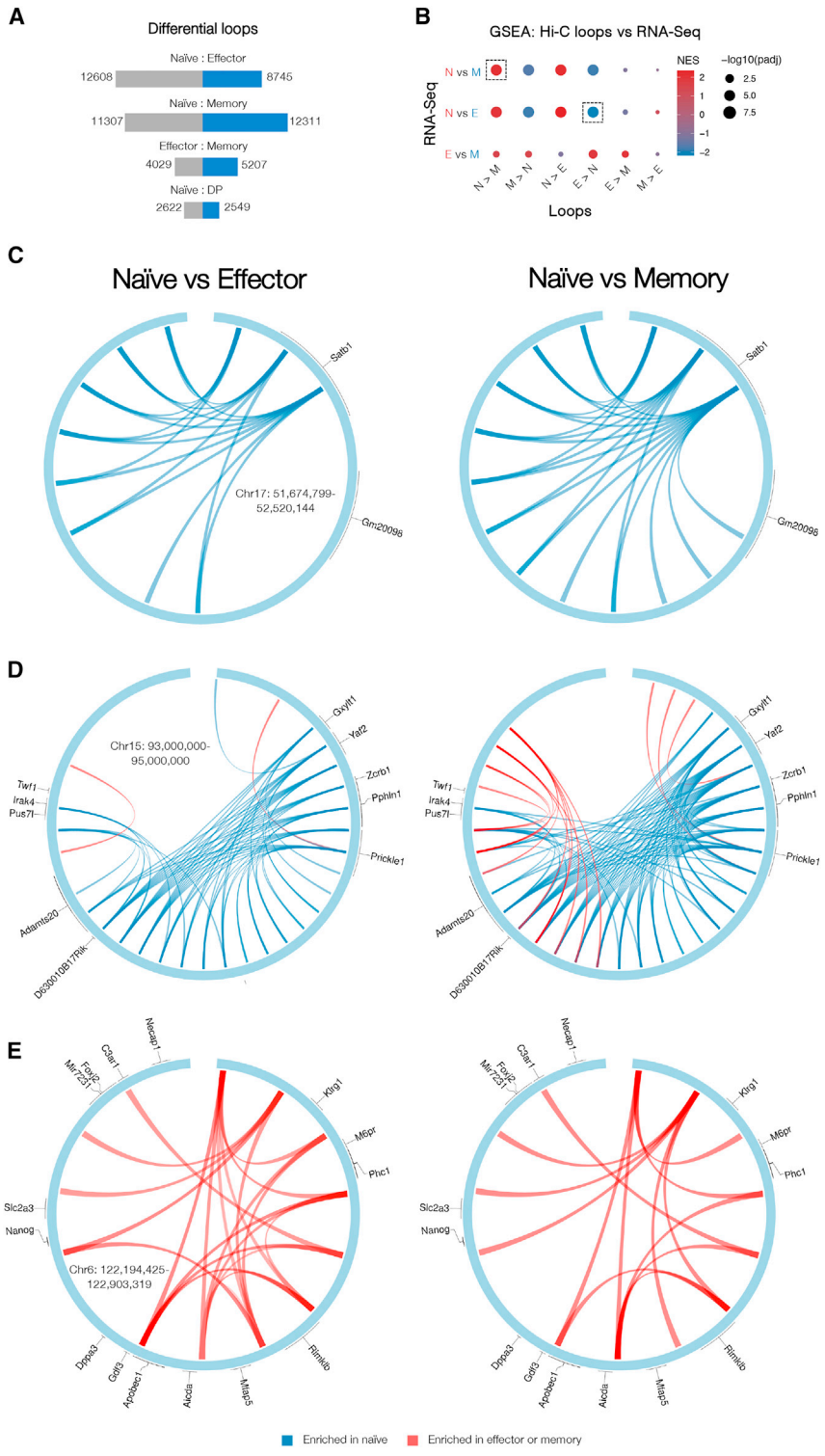

Figure 3. Loss and gain of *cis*-regulatory interactions underscores CTL differentiation-state-specific gene transcription profiles

(A) Numbers of *cis* interactions unique to each differentiation state, determined by pairwise comparisons using multiHiCcompare (50 kb resolution, 0.05 false discovery rate).

(B) GSEA analysis comparing genes connected by loops enriched in one condition over another (y axis), against RNA-seq data derived from matching samples.[8] Circle sizes reflect adjusted p values (−log10) and color represents normalized enrichment score (NES), with red indicating enrichment versus the first RNA-seq condition listed in pairwise comparison, and blue indicating enrichment is the second RNA-seq condition listed.

(C–E) Examples of loci where loops were lost and gained upon differentiation (blue loops are present in naive over effector or memory; red loops are gained on differentiation). Locus coordinates (base pairs) are shown within the naive versus effector circus plot.

gained interaction frequency included genes involved in tolerance/co-stimulation including *Cd86*, *Icos*, and *Cblb*, and the killer like receptors *Klra1*, *Klra2*, and *Klrg1*, while examples of genes within regions that lost interaction frequency include *Sox5* and *Tgfbr2* (Table S2). In total, we found the greatest number of domain changes between naive and effector (144) and naive and memory (69) samples, with relatively few gross differences separating effector and memory (11) (Figure 2L). These data are consistent with the close clustering of effector and memory in our MDS analysis (Figure 2A), suggesting a gross change in genome structure following antigen exposure, which is maintained into CTL memory.

Chromatin looping dynamics underscore CTL differentiation states

To further understand how looping dynamics influence CTL gene transcription following virus infection, we identified loops that were lost or gained following infection using the multiHiCcompare package.[41] We identified between 5,171 and 23,618 differential loops when samples were compared pairwise, with the largest number separating naive from memory (23,618), and naive from effector (21,353), while effector and memory were separated by considerably fewer differences (9,416), again suggesting that these states share a similar genome organization (Figure 3A; see Table S3 for loops called and gene assignments). Interestingly, naive and DP samples had fewer differences (5,171) than naive and effector, or naive and memory, consistent with our MDS analysis (Figure 3A). An aggregate peak analysis demonstrated that unique loops called naive and effector states were indeed enriched in those states (Figure S2A). Moreover, there was no difference in

loop length distributions between the differentiation states (Figure S2B).

Next we assigned loop ends to the nearest gene (methods) and performed Gene Set Enrichment Analysis (GSEA) to determine whether loss and gain of loops was associated with changes in gene transcription (Figure 3B). Overall, we found a strong correspondence between differentiation-state-specific loss and gain of Hi-C contacts and a corresponding loss and gain of gene transcription. For example, we found that loops enriched in naive over effector CTLs, and naive over memory CTLs were associated with genes transcribed more strongly by naive than effector CTLs (normalized enrichment score [NES] = 2.36), and naive than memory CTLs, respectively (NES = 2.08; relevant comparisons indicated by dashed boxes). This pattern of altered chromatin interactions tracking with changes in gene expression was also observed in our earlier study[42] using a different infection model and effector subsets, suggesting that this phenomenon does not depend on infection type and reflects intrinsic mechanisms associated with $CD8^+$ T cell differentiation programs.

Next we inspected individual gene loci to further understand how fine-scale looping dynamics reflected gene transcription, finding that broadly, loss and gain of looping corresponded with loss and gain of gene expression, respectively. For instance, loci encoding *Satb1*, *Prickle1,* and *Sox4*—genes associated with maintenance of stemness and quiescence, which are strongly downregulated following the transition of naive $CD8^+$ T cells into the effector/memory states (Figures 2G–2I)—have dense looping structures in naive $CD8^+$ T cells, that are lost on differentiation to effector or memory (Figures 3C and 3D and S2C; blue ribbons indicate loops present in naive over effector (left panels), or naive over memory (right panels), while red ribbons are gained following differentiation of naive $CD8^+$ T cells into effector or memory states). Conversely, loci encoding genes that are expressed following naive $CD8^+$ T cell activation (*Klrg1* – Figure 3E); *GzmA* and *GzmK* (Figure S2D – top panel; and *Ccl3*, *Ccl4*, *Ccl5*, *Ccl6*, and *Ccl9* – bottom panel; Figure S2E) are characterized by increased looping following differentiation of naive T cells to effector or memory. Noticeably, looping dynamics following differentiation of naive $CD8^+$ T cells to effector were largely shared with those following differentiation of naive cells to memory, suggesting a mechanism for the rapid recall of effector function following reactivation of memory CTLs, and this was consistent with the close grouping of effector and memory states in our MDS plot (Figure 2A).

Chromatin loops are enriched for differentiation-state-specific transcriptional enhancers

We next aimed to understand the mechanisms by which differentiation-specific chromatin loops imparted transcriptional programs characteristic of the different $CD8^+$ T cell states. We found that naive-specific chromatin loops were enriched for accessible chromatin (measured by ATAC-seq), but the same regions in effector CTLs were not (Figure 4A). In contrast, effector chromatin loops were enriched for open chromatin in effector CTLs, but the same regions in naive T cells were not. Moreover, accessible chromatin enrichment patterns for the same regions in memory T cells were very similar to those found for effector T cells, again suggesting that a similar chromatin structure underscores the capacity of memory CTLs to elicit rapid effector function. Moreover, chromatin loops enriched in naive over effector T cells were enriched for a histone PTM signatures indicative of active and poised transcriptional enhancers ($H3K4me1^+$ $H3K4me2^{+3}$) and vice versa (Figure 4B). Further, these regulated loops were enriched specifically for regulated enhancers, but not constitutive enhancers ($H3K4me1^+$ $H3K4me2^+$ enhancers shared by naive and effector states) (Figures 4A and 4B). Indeed, upon inspection of individual loci, looping interactions largely connected regions of the genome that were decorated with chromatin features characteristic of active and poised regulatory elements (Figures 4C and 4D), including H3K4me1, H3K4me2, H3K4me3, and increased chromatin accessibility as measured by ATAC-seq (dark blue, light green, dark green, and red tracks, respectively), although interestingly, some loops did not appear to connect obvious regulatory regions.

We observed that some genes were connected by multiple enhancers; however, this did not appear to result in increased gene transcription (Figure S3A). Further, while interactions between enhancers and gene promoters were common, we also observed promoter-promoter interactions as reported previously for human $CD4^+$ T cells (for instance, at the *Sox4* locus; Figure S2C).[44] Indeed, when interactions were stratified by the genomic elements they were connected to (Figure 4E), we found that loops connecting promoters to promoters were ~2-fold more abundant than loops connecting promoters to enhancers (60% versus 30% of loops, respectively), and this was true both of loops enriched in naive over effector ("naive loops") and vice versa ("effector loops"). By comparison, loops connecting enhancers to enhancers, were far less frequent (~6% of interactions). This is in line with observed frequencies using ChIA-PET to assess chromatin:chromatin interactions in resting primary human $CD4^+$ T cells.[44] While promoter:promoter interactions have been proposed to reflect co-regulation of linked genes,[44] we did not observe a correlation between transcription of genes linked differentiation-state-specific promoter:promoter interactions (Figure S3B) suggesting this is not a major mechanism of transcriptional control in mouse virus-specific $CD8^+$ T cells.

Our data show that the unique chromatin looping observed in either naive or effector/memory virus-specific $CD8^+$ T cells was enriched for differentiation-state-specific TEs. To gain molecular insights into how regulated TE utilization between naive and effector/memory states may influence distinct transcriptional signatures, we examined TF enrichment based on curated publicly available lymphocyte CHIP-seq datasets.[43] This showed that naive-T-cell-specific enhancers found to interact with gene promoters or other enhancers were enriched for binding of TCF1 and FOXO1, which have roles in maintenance of T cell stemness and quiescence (Figure 4F).[19–21] By contrast, effector-specific enhancers connected to effector-specific regulatory regions were enriched for binding of TFs such as TBX21 (TBET), IRF4, and PRDM1 (BLIMP1), which have roles in terminal effector differentiation (Figure 4F).[15–18] Taken together, these data suggest that the dynamics of *cis*-regulatory interactions underscore instillation of differentiation-specific transcriptional programs within $CD8^+$ T cells, largely by connecting genes with enhancers bound by key TFs.

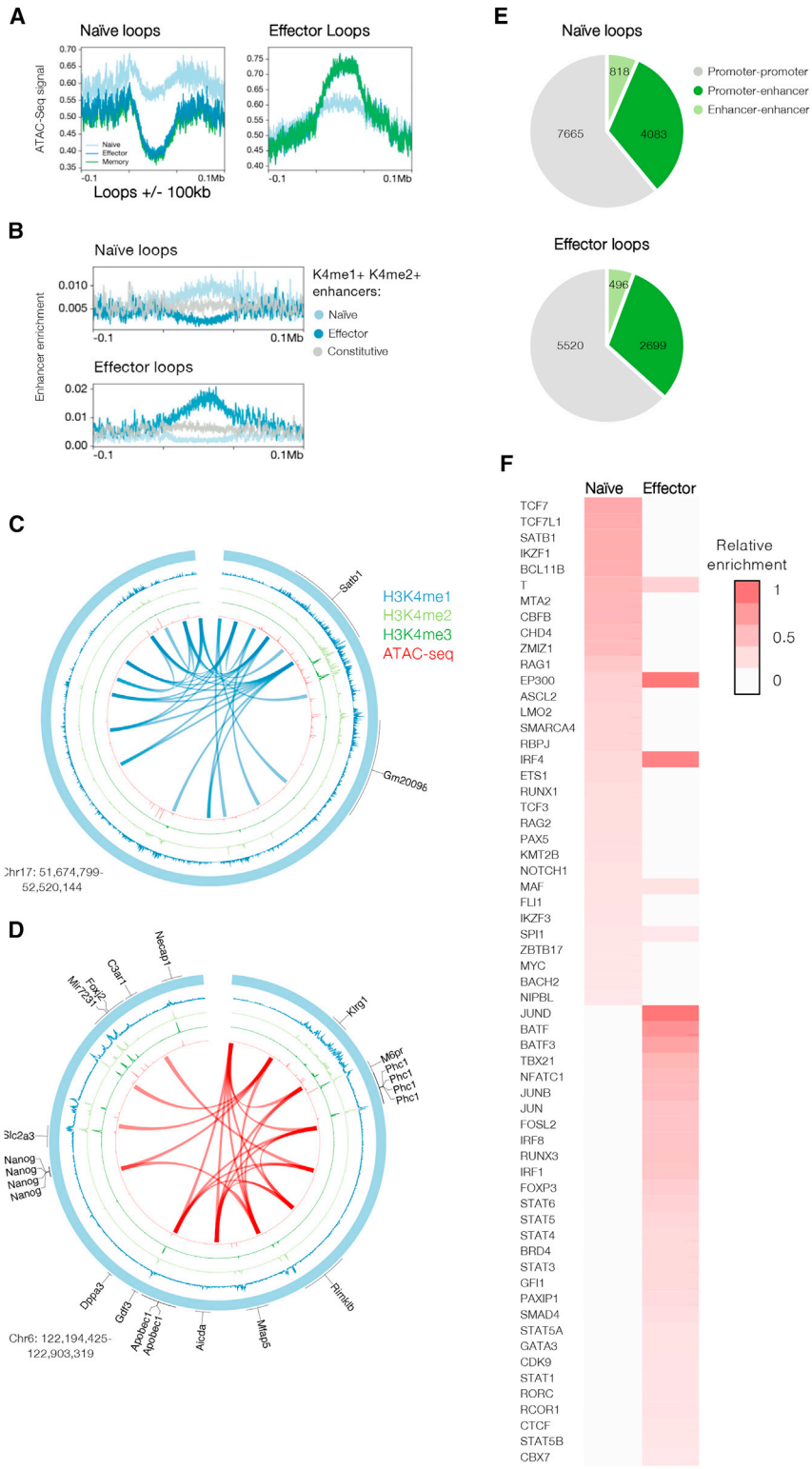

Figure 4. Hi-C loops border active regions containing differentiation-state-specific enhancers

(A) ATAC-seq signal (log2) indicating open chromatin within and surrounding loops that are present in naive but not effector CTLs, or vice versa. Loops are scaled to occupy 100 kb, and ATAC-seq signal is shown for 100 kb up and downstream of the loop borders.

(B) Enrichment of active and poised (H3K4me1$^+$ H3K4me2$^+$) transcriptional enhancers that occur in naive CD8$^+$ T cells but not effector T cells within loops that occur in naive but not effector CD8$^+$ T cells (upper panel) and vice versa (lower panel). Enhancers present in both naive and effector T cells (constitutive) are shown for both comparisons.

(C and D) *Cis* interactions connect gene regulatory elements. Circos plots show the gene neighborhood of *Satb1* (C) and *Klrg1* (D) in naive and effector OT-1 CTLs, respectively. Tracks in order from outside to the center are genes, H3K4me1 (blue), H3K4me2 (light green), H3K4me3 (dark green), ATAC-seq (red), Hi-C interactions (naive over effector CTLs [B] and effector over naive CTLs [C]) shown as ribbons. Locus coordinates are given on the bottom left of the plot.

(E) Summary of regions connected by loops present in naive but not effector T cells, or vice versa.

(F) Enrichment of transcription factor binding at TEs unique to naive or effector,[3] that were connected by loops enriched in naive over effector, or vice versa. Enrichment was performed using curated transcription factor CHIP-seq data through the CistromeDB Toolbox.[43]

BAHC2 enforces the naive-T-cell-specific looping architecture

BACH2 and SATB1 are both chromatin-binding proteins that are highly expressed in naive CD8$^+$ T cells and downregulated upon effector/memory CD8$^+$ T cell differentiation.[22,45] Interestingly, BACH2 and SATB1 binding sites were only enriched within naive-specific chromatin loops (Figure 4F), suggesting they may play a role in maintaining state-specific chromatin architecture within naive CD8$^+$ T cells. To understand if and how these TFs impact the looping architecture of naive T cells, *in situ* Hi-C was performed on sort purified naive CD8$^+$ T cells from mice with either a point mutation in the DNA binding domain of SATB1 that abrogates DNA binding[45,46] (*Satb1*$^{m1Anu/m1Anu}$) or with a T cell-specific BACH2 deletion (*Bach2*$^{fl/fl}$ × *Cd4 Cre* mice; *Bach2*$^{-/-}$ herein[22]; library statistics in Table S1).

To broadly assess changes in genome architecture, an MDS analysis was performed (as in Figure 2A), comparing these datasets with the wild-type (WT) naive, effector, and memory datasets described above (Figure 5A). We found that while the *Satb1*$^{m1Anu/m1Anu}$ datasets overlapped the naive WT, the *Bach2*$^{-/-}$ datasets clustered more closely with effector, suggesting that deletion of BACH2 within naive CD8$^+$ T cells is sufficient to remodel higher-order chromatin structures to resemble those observed after effector CTL differentiation. Consistent with this, a pairwise comparison of loops lost and gained between naive WT and *Bach2*$^{-/-}$ CD8$^+$ T cells identified ~17,583 differences (Figure 5B), which was similar to the number of different loops that identified between WT naive and effector (~21,000; Figure 3A) CD8$^+$ T cells, while far fewer loops (4,249) separated virus-specific effector and naive *Bach2*$^{-/-}$ CD8$^+$ T cells. Consistent with the differential loop and MDS analyses, GSEA analysis showed that genes associated with loops gained in naive *Bach2*$^{-/-}$ CD8$^+$ T cells relative to naive WT CD8$^+$ T cells, are more highly transcribed in effector than (WT) naive T cells (NES 2.79) (Figure 5C). Comparison of RNA-seq data from naive *Bach2*$^{-/-}$ CD8$^+$ T cells with WT naive and effector transcriptomes showed that naive *Bach2*$^{-/-}$ cells do indeed have upregulated expression of transcripts characteristic of effector CTLs, including *Ccl5*, and *GzmA* and *GzmB* (Figure S4; Table S4).[22] Noticeably, we have also previously observed that chromatin changes induced by *Bach2* deletion were similar to activated T cell subsets with greater differentiation potential.[42] Thus, deletion of *Bach2* within naive CD8$^+$ T cells shifts the chromatin architecture and transcriptional profile of related genes to resemble antigen experienced CD8$^+$ T cell subsets.

Consistent with BACH2 having a role in maintaining CD8$^+$ T cells in a naive state, we found that the locus encoding *Foxo1*, which is itself required to enforce T cell naivety[20] was reorganized in naive *Bach2*$^{-/-}$ CD8$^+$ T cells, with both loss (blue) and gain (red) of loops relative to the WT (Figure 5D). Indeed, *Bach2*$^{-/-}$ cells showed loss of a loop connecting the *Foxo1* promoter and a downstream non-coding element (Figure 5D), suggesting that BACH2 maintains T cell naivety in part by driving FOXO1 expression. Importantly, we also found a loss of looping at the *Tcf7* and *Lef1* loci and gain of loops at the *Prdm1* (BLIMP1), *Tbx21* (TBET), *Zeb2*, and *Nfatc4* loci, suggesting a loss of naive potential and engagement of the effector CTL transcriptional program (Table S3). Consistent with this, the *Klrg1* encoding locus also underwent large-scale reorganization with a gain in loops in naive *Bach2*$^{-/-}$ compared with WT naive CD8$^+$ T cells (Figure 5E). Importantly, the loops gained at the *Klrg1* locus after deletion of *Bach2* were largely identical to those gained on differentiation of WT naive T cells to an effector and memory state following virus infection (Figure 3E). Finally, loops that were acquired in *Bach2*$^{-/-}$ T cells occurred in regions that harbor enhancers that are active and poised (H3K4me1$^+$ H3K4me2$^+$) in effector but not naive CD8$^+$ T cells (Figure 5F). Thus, taken together, these data indicate that BACH2 is essential for maintenance of CD8$^+$ T cell naivety because it enforces a looping architecture that maintains naive T cell quiescence and stemness functions, while blocking engagement of effector transcriptional programs.

A distal role for SATB1 in maintenance of a naive-specific looping architecture

Given that SATB1 binding sites were enriched within naive-specific enhancers (Figure 4E), and our recent data demonstrating that naive *Satb1*$^{m1Anu/m1Anu}$ CD8$^+$ T cells have an activated phenotype,[45] this suggested that SATB1 may also play a role in ensuring CD8$^+$ T cell naivety via chromatin organization. To understand this further, a pairwise comparison of looping architectures was performed on WT naive and *Satb1*$^{m1Anu/m1Anu}$ naive Hi-C datasets described in Figure 5A. We found 562 differential loops in this comparison (Figure 6A; Table S3), much fewer than that described for *Bach2*$^{-/-}$ (Figure 5B) and comparisons between virus-specific CD8$^+$ T cell datasets (Figure 3A). Next, we performed GSEA analysis to determine whether changes in the loop architecture observed might underscore the activated phenotype of naive CD8$^+$ T cells *Satb1*$^{m1Anu/m1Anu}$ mice.[45] Genes associated with loops gained in naive *Satb1*$^{m1Anu/m1Anu}$ CD8$^+$ T cells (relative to the WT) were compared with RNA-seq data from naive and influenza-virus-specific effector OT-1 T cells (Figure 6B).[45] Indeed, we found that genes associated with *Satb1*$^{m1Anu/m1Anu}$-specific loops tended to be upregulated in effector T cells relative to naive (NES 1.49), indicating that the altered looping architecture was likely driving the activated transcriptome and phenotype of *Satb1*$^{m1Anu/m1Anu}$ cells.

To understand this further, we inspected the dynamics of looping loss and gain at individual gene loci. We found that at the type 1 chemokine locus (encoding *Ccl3*, *Ccl4*, *Ccl5*, *Ccl6,* and *Ccl9*), there was a loss of loops in naive *Satb1*$^{m1Anu/m1Anu}$ T cells, relative to naive WT, despite *Ccl5* being upregulated in the latter (Figure 6C). Moreover, closer inspection of contact matrices confirmed a partial loss of contact frequency across the region in the *Satb1*$^{m1Anu/m1Anu}$ T cells, which also appeared to occur in effector CTLs together with a "spreading" of the zone of contacts (Figure 6D). Thus, it appeared that acquisition of *Ccl5* transcription within effector CTLs required a gross and stepwise remodeling of looping architecture, with *Satb1*$^{m1Anu/m1Anu}$ T cells having an architecture and transcriptional profile intermediate between WT naive and effector.

Finally, fewer alterations to the *Satb1*$^{m1Anu/m1Anu}$ looping architecture relative to that observed in the *Bach2*$^{-/-}$ dataset (Figures 6A and 5B, respectively) suggested that SATB1 plays a more minor role in maintaining naive CD8$^+$ T cell chromatin architecture compared with BACH2. Indeed, inspection of the

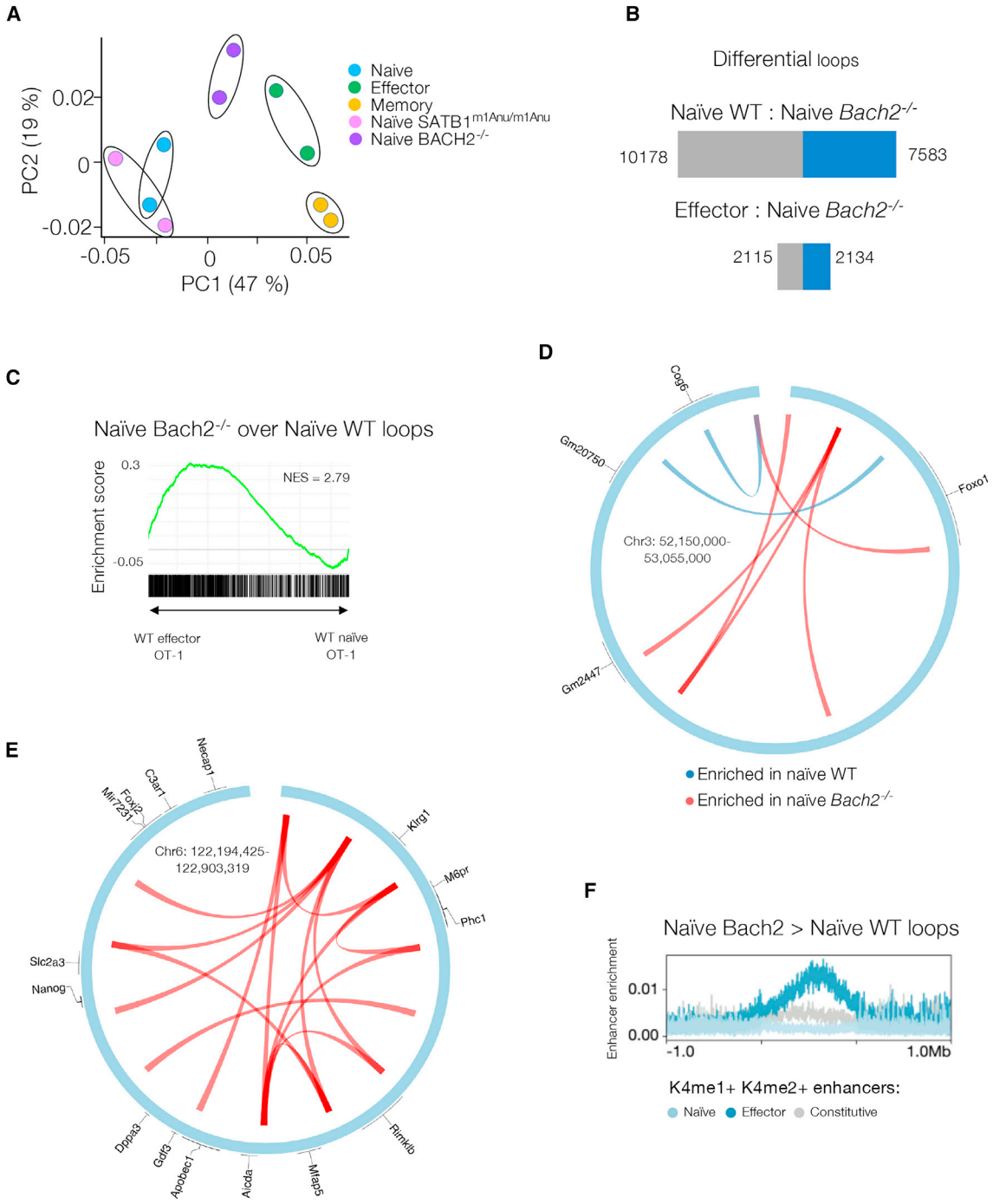

Figure 5. BACH2 enforces a naive chromatin architecture

(A) MDS plot showing relationship between naive *Bach2*$^{-/-}$ and naive *Satb1*$^{m1Anu/m1Anu}$ CD8^{+} T cells (described in Figure 7), Hi-C samples, and naive, effector, and memory OT-1 CD8^{+} T cells.

(B) Loss and gain of *cis* interaction in naive *Bach2*$^{-/-}$ CD8^{+} T cells in comparison with WT naive- and virus-specific OT-1 CD8^{+} T cells.

(C) GSEA analysis comparing genes connected by loops gained in naive *Bach2*$^{-/-}$ CD8^{+} T cells relative to naive WT CD8^{+} T cells against RNA-seq data derived from naive and effector CTLs samples.[8] p values and normalized enrichment score (NES) are shown.

(D and E) Examples of changes in looping architecture in naive *Bach2*$^{-/-}$ CD8^{+} T cells relative to naive WT CD8^{+} T cells (blue loops are enriched in WT naive over naive *Bach2*$^{-/-}$ CD8^{+} T cells and red loops are enriched in naive *Bach2*$^{-/-}$ CD8^{+} T cells over WT).

(F) Loops that occur in naive *Bach2*$^{-/-}$ CD8^{+} T cells but not WT naive CD8^{+} T cells are enriched for active and poised (H3K4me1^{+} H3K4me2^{+}) transcriptional enhancers that occur in effector CD8^{+} T cells but not naive T cells. Constitutive enhancers are defined as present in both effector and naive.

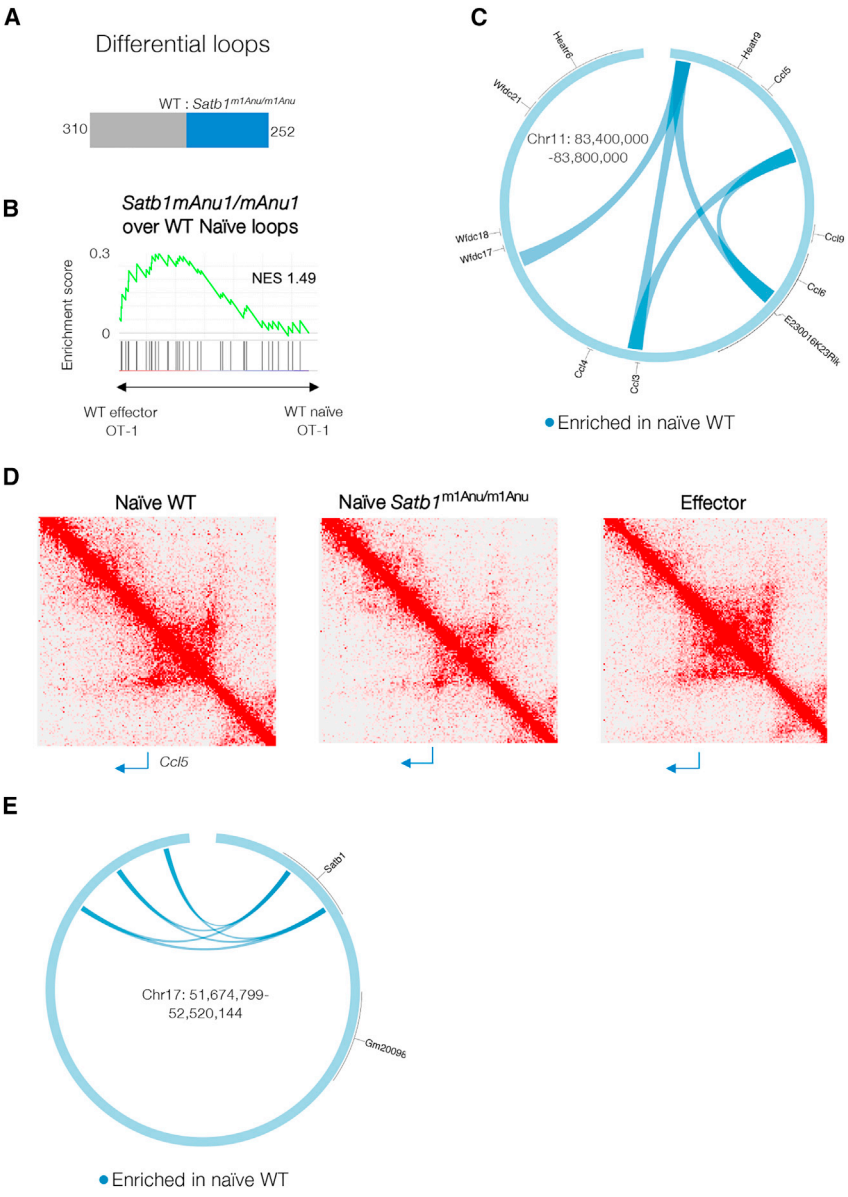

Figure 6. SATB1 maintains CD8⁺ T cell naive chromatin architecture

(A) Loss and gain of *cis* interactions in naive *Satb1*$^{m1Anu/m1Anu}$ CD8⁺ T cells in comparison with WT naive OT-1 T cells.

(B) GSEA analysis comparing genes connected by loops gained in naive *Satb1*$^{m1Anu/m1Anu}$ CD8⁺ T cells relative to naive OT-1 T cells against RNA-seq data derived from naive and effector OT-1s.[7] Normalized enrichment score (NES) is shown.

(C) Loops lost at the type 1 chemokine locus in naive *Satb1*$^{m1Anu/m1Anu}$ CD8⁺ T cells relative to naive OT-1 cells.

(D) Hi-C contact maps showing the *Ccl5* encoding locus in naive OT-1, *Satb1*$^{m1Anu/m1Anu}$ naive, and effector OT-1 CTLs.

(E) Loops lost at the *Satb1* locus in naive *Bach2*$^{-/-}$ CD8⁺ T cells relative to naive OT-1 cells.

looping architecture at the *Satb1* locus in the naive *Bach2*$^{-/-}$ dataset showed a partial loss of loops present in naive CD8⁺ T cells (compare Figures 6E and 3C, respectively), while the architecture of the *Bach2* locus was not altered in the *Satb1*$^{m1Anu/m1Anu}$ dataset (data not shown). Thus, taken together, these data suggest that the role that SATB1 plays in maintaining naive CD8⁺ T cell chromatin architecture is likely to be downstream of BACH2.

Altered chemokine expression in mice following deletion of *cis* interacting elements mapped by Hi-C

Having found that the dynamics of loss and gain of *cis* chromatin interactions broadly described the installation and maintenance of T cell differentiation-state-specific transcriptional programs (Figures 3A and 3B), we next asked whether these interactions were necessary drivers of those programs. We had previously used ChIP-seq to identify putative transcriptional enhancers of *Ccl5* located at −5 kb and −20 kb region upstream of the *Ccl5* promoter.[3] Given that differentiation from naive to effector T cell states corresponded with acquisition of chromatin contacts at the *Ccl5* locus (Figure 6D), we performed virtual chromosome confirmation capture (4C) at 5-kb resolution, starting at the *Ccl5* TSS, to determine whether the acquired contacts involved may explain acquisition of CCL5 expression upon effector differentiation (Figure 7). Indeed, we found an increased interaction frequency between the *Ccl5* promoter and a region spanning ~20 kb upstream in effector cells (Figure 7A), which correlated with the position of the −5 and −20 kb *Ccl5* enhancers we had previously identified,[3] suggesting that loops connecting the *Ccl5* promoter and upstream regulatory elements are installed upon T cell activation to license *Ccl5* transcription. To assess the functional impact of these interactions on *Ccl5* transcription, we used CRISPR-Cas9 genome targeting to generate two separate mouse lines with deletions at the *Ccl5* −5 kb or −20 kb enhancers (Δ−5 kb and Δ−20 kb lines, herein; Figure 7B). The Δ−5 kb and Δ−20 kb lines and WT C57BL/6 controls were infected intranasally with influenza A/HKx31 virus, and lymphocytes from bronchiolar lavage fluid (BAL), spleens and draining lymph node (mediastinal lymph node; MLN) were sampled 10 days post infection, and chemokine expression was assessed by ICS. Further, the body weight of mice was monitored throughout the course of the infection, where we found that both mutant lines lost significantly more weight than the WT, with the Δ−20 kb line having the most significant weight loss (days 3–9 post infection; $p < 0.01$; Figure S5A). We found that within each tissue, the Δ−5 kb deletion nearly completely

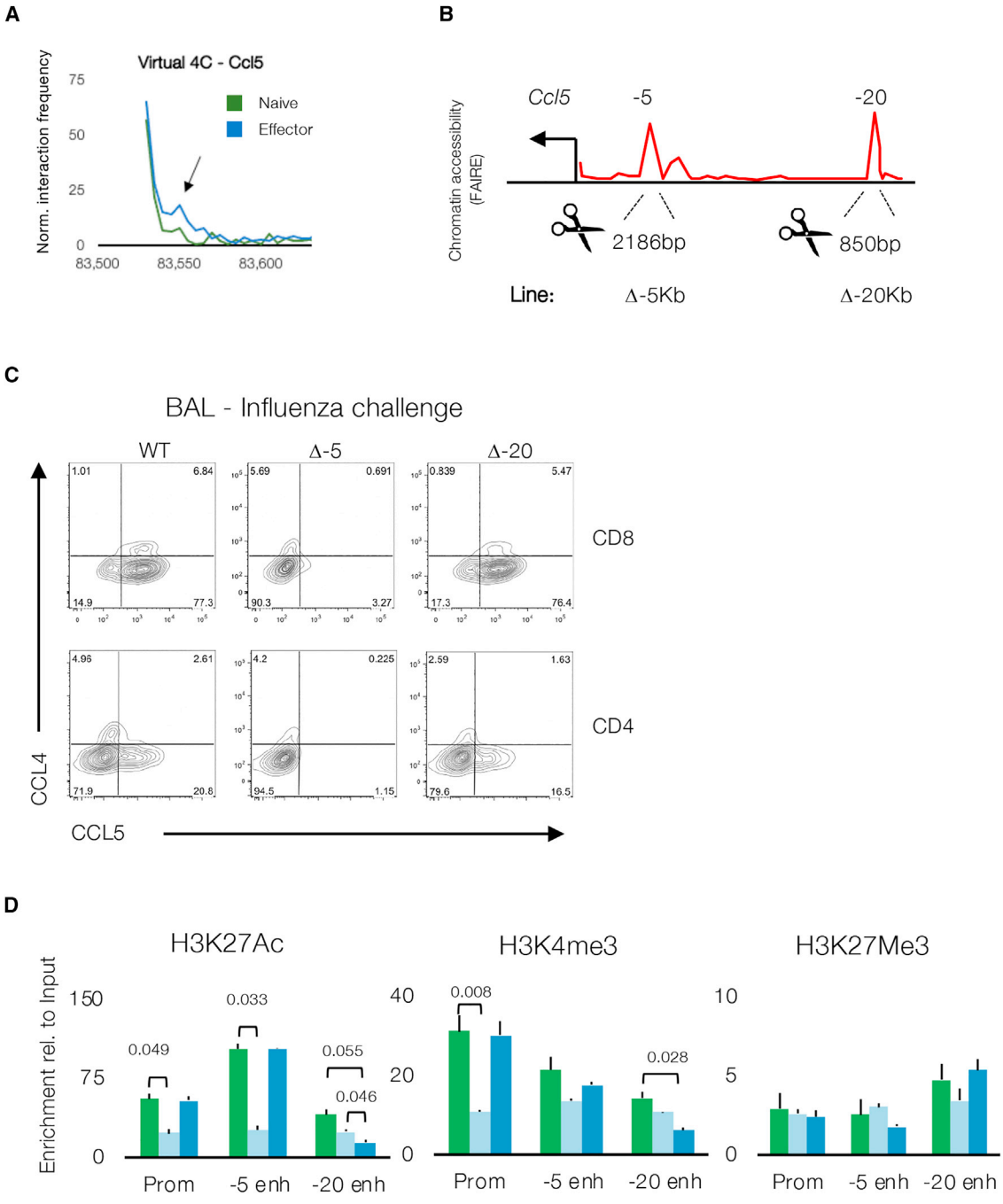

Figure 7. Altered chemokine expression in mice following deletion of *cis* interacting elements mapped by Hi-C

(A) Identification of interactions between the *Ccl5* gene promoter and previously identified transcriptional enhancers at −5 kb and −20 kb from the *Ccl5* transcription start site.[3] Data are presented as a virtual 4C plot, showing naive and effector Hi-C data, with the arrow indicating a zone of increased interaction in effector CTLs.

(B) Chromatin accessibility data (mapped by FAIRE) in effector CTL, showing the positioning of CRISPR deletions made in separate mouse lines to remove the −5 and −20 transcriptional enhancers.

(C) Wild-type and enhancer deletion mice were infected intranasally with 10^4 pfu A/HKx31influenza virus, and lymphocytes were collected from the bronchiolar lavage (BAL) fluid on d10 for analysis by flow cytometry to assay CCL4 and CCL5 expression in $CD8^+$ and $CD4^+$ T cells.

(D) Reduced H3K27Ac at the *Ccl5* locus in *in vitro* cultured enhancer deletion effector CTLs. Naive CTL from WT (blue) and −5 (red) and −20 (green) enhancer deletion mice were stimulated with plate-bound αCD3 and αCD28 and cultured for 5 days before ChIP assays were performed to measure histone acetylation at the promoter and enhancers of *Ccl5*. Data are pooled from three independent cultures, and error bars are SEM. Data are expressed relative to a total input, and statistical significance was determined using a two-tailed t test.

abolished CCL5 production, both by virus-specific CD8$^+$ T cells and CD4$^+$ T cells, while surprisingly, the Δ−20 kb deletion did not impact CCL5 expression in either subset, despite this line having the most significant weight loss following influenza challenge (Figures 7C and S5B). Thus, these data demonstrate that acquisition of the loop connecting the −5 enhancer with the CCL5 promoter is required to enable CCL5 expression within effector CTLs and CD4$^+$ T cells.

To understand the mechanism by which deletion of loop ends impacts CCL5 expression, ChIP was performed on *in vitro* effector CTLs to probe the chromatin composition of regions immediately adjacent to the −5 kb and −20 kb deletions, as well as the *Ccl5* promoter (H3K4me3 and H3K27Ac, which mark active chromatin, and H3K27me3, which marks repressed chromatin; Figure 7D). In WT CTLs, we found enrichment of H3K4me3 and H3K27Ac at all three regions, while H3K27me3 was distributed evenly across the locus, albeit at low enrichment levels. In contrast, Δ−5 kb CTLs had diminished levels of the permissive modifications across the locus, while Δ−20 kb CTLs had a minor reduction in levels of the permissive modifications specifically adjacent to the deletion site. Thus, these data suggested that deleting loop ends impacts the ability of the *Ccl5* locus to acquire a transcriptionally permissive chromatin following T cell activation, consistent with our finding that differentiation-specific loops demarcate regions of open chromatin capable of regulating T cell gene-specific function (Figure 4A).

DISCUSSION

Changes in CD8$^+$ T cell differentiation state drive pathogen clearance and immune memory formation through transcriptional reprogramming.[5,8] This process involves regulated enhancer usage,[8,11,12,32] TF binding,[15–18] and chromatin composition,[8,14] yet the factors interplay of these factors in the 3-dimensional space of the nucleus remains poorly understood. Our findings demonstrate that chromatin looping orchestrates transcriptional reprogramming where TEs, TFs, and genes converge to establish and maintain transcriptional programs. Importantly, higher-order chromatin structures in effector and memory CD8$^+$ T cells share similarities and associate with effector/memory transcriptional signatures. These data suggest that the rapid effector function exhibited by memory CTLs is underpinned by reorganization of chromatin architecture from a naive to effector/memory state.

Traditionally, TADs maintain discrete functional genomic compartments with invariant boundaries across cell types.[35–38,47] Our data suggest dynamic TAD boundary repositioning, during CD8$^+$ T cell differentiation, particularly at fine resolutions. This aligns with recent data on TCF-1/CTCF-dependent TAD boundaries reorganization in thymocytes, enabling new interactions between gene loci and neighboring regulatory elements.[39] Fine-scale chromatin topology changes in virus-specific CD8$^+$ T cells upon activation appear to resemble subTAD structures.[33] We have previously demonstrated that differences in fine-scale chromatin topology between naive CD8$^+$ T cells and precursor effector and memory cells is dependent on CTCF.[42] Whether the changes observed represent formation of subTADs or actual *de novo* TADs remains uncertain.

Naive CD8$^+$ T cells possess distinct genome architecture compared with effector or memory CD8$^+$ T cells, with large-scale architectural changes required for lineage-specific function. In contrast, virus-specific effector and memory CD8$^+$ T cell genomes exhibit similar genome architecture. This aligns with previous findings of open chromatin at effector loci in resting memory T cells.[8,48–50] Thus, the rapid response of memory CD8$^+$ T cells without further differentiation is underpinned by stable higher-order chromatin structures that poise CD8$^+$ T cell effector genes for transcription.

We observed CD8$^+$ T cell differentiation-state-specific connections between TEs and gene promoters (Figure 3). Additionally, promoter:promoter interactions also differed across cell states, possibly reflecting transcriptional hub formation within the same chromatin compartments. It has been proposed that such interactions are a mechanism to ensure co-regulation of functionally important genes in primary human CD4$^+$ T cells, although the same study found that this mechanism was not employed by a second cell type.[44] We did not find evidence of significant co-regulation of promoter:promoter connected genes in our CD8$^+$ T cell datasets suggesting distinct regulatory mechanisms may be used by CD4$^+$ and CD8$^+$ T cells, or differences in human and mouse T cell biology. It could be establishment of promoter:promoter interactions within these molecular neighborhoods may reflect their close proximity with gene-specific transcription requiring the further molecular factors, such as specific TFs, that target individual genes within these molecular neighborhoods to drive transcription.

Our analysis demonstrated a clear delineation of TF binding sites enrichment within the unique chromatin looping architecture that distinguished naive and effector/memory CD8$^+$ T cell states. TFs, such as TCF-1 and AP1 factors, contribute to chromatin spatial organization in central memory CD8$^+$ T cells, with TCF1 ablation resulting in an inability to engage transcription of genes required for secondary expansion and metabolic reprogramming.[51,52] These observations imply that genome architecture is not sufficient to instruct cell-type-specific gene transcription, but rather, TFs serve to preconfigure the spatial organization of chromatin to transcriptionally poise appropriate genes for rapid activation following secondary challenge. Hence, the unique chromatin landscapes formed within naive and effector/memory CD8$^+$ T cells form an important scaffold that is read by specific TFs indicating their role in determining lineage-specific differentiation.

We found numerous regulated contacts with "Gm" genes (Table S3), many encoding long non-coding RNAs (lncRNAs).[53] Transcription of lncRNAs has been reported to be involved in spatial repositioning of genomic regions to facilitate gene transcription.[54,55] Transcription of the lncRNA, *ThymoD*, during T cell development is essential for genome repositioning and remodeling of the *Bcl11b* gene locus to initiate gene transcription, and commitment of T cell progenitors to the T cell lineage.[56] Thus, our findings suggest that lncRNA expression may have a broader role in regulating chromatin architecture than is currently appreciated and may indeed be an important regulator of CD8$^+$ T cell differentiation.

Surprisingly, deleting *Bach2* led to significant remodeling of the naive CD8$^+$ T cell genome, making it architecturally similar

to effector CTL genomes. This suggests that CD8$^+$ T cell differentiation is largely autonomous, with BACH2 maintaining naivety by preventing loop formation required for effector transcriptional programming. These findings support studies showing that BACH2 restrains CTL differentiation by competing with AP-1 factors for enhancers binding in naive T cells,[22,57] which, when activated, drive terminal CD8$^+$ T cell effector differentiation.[22] The mechanisms behind how and why BACH2 deficiency promotes effector T cell differentiation in the absence of infection remains to be determined. Interestingly, Quon and colleagues[42] found CTCF enrichment upstream of regions with altered chromatin interactions after *Bach2* deletion, hinting at a potential collaboration between BACH2 and CTCF in regulating chromatin interactions. In any case, these observations highlight that BACH2 loss allows extensive remodeling of the naive genome and loss of CD8$^+$ T cell naivety.

In line with the BACH2 findings showing specific TFs maintain naive CD8$^+$ T cell chromatin architecture, we observed that mutating SATB1 partially reconfigured the genome structure in naive CD8$^+$ T cells. This supports an earlier study highlighting the role of SATB1 as a chromatin organizer in CD4$^+$ T cells.[58] The Satb1$^{m1Anu/m1Anu}$ mutation led to effector-like chromatin organization at the *Ccl4*/*Ccl5* locus, consistent with transcriptional data showing early activation hallmarks in naive CD8$^+$ T cells from *Satb1*$^{m1Anu/m1Anu}$ mice, including increased *Ccl4* and *Ccl5*[45] expression. Interestingly, unlike the *Bach2* mutant, the *Satb1*$^{m1Anu/m1Anu}$ mutation only induced partial chromatin remodeling, despite binding sites for both TFs observed in naive-specific chromatin loops. This suggests that SATB1 and BACH2 may operate at different regulatory levels in maintaining naive CD8$^+$ T cell genome architecture. Furthermore, the observation that the *Satb1* locus is remodeled in the *Bach2* mutant, but not vice versa, and the less pronounced changes in genome architecture in the *Satb1* mutant, indicate that SATB1 likely acts downstream of BACH2 and may fine-tune genome structure.

A recent study showed that compound deletion of *Lef1* and *Tcf7* within naive CD8$^+$ T cells resulted in an altered genome architecture and transcriptome.[59] These alterations affected various levels of genome organization, including at the level of compartments, TAD structures, and looping. Notably, the transcriptional changes included increased expression of effector program genes within naive cells, only with other genes typically expressed in other lymphocytes (such as B cells and NK cells) and myeloid lineage cells (including granulocytes). While it remains unclear whether these TFs directly mediate chromatin spatial organization or regulate expression of chromatin organizing proteins, these studies underscore how specific TFs play a role in maintaining T cell naivety and lineage fidelity by influencing different aspects of genome structure.

Our data highlight a crucial and unique distinction between naive and effector/memory CD8$^+$ T cell states, namely the spatial and looping interactions observed within higher-order chromatin structures. Moreover, our data point to key chromatin-binding proteins as providing the molecular restraint that is actively enforced in naive CD8$^+$ T cell, which is distinct from the "rapid-fire" capacity of effector/memory CD8$^+$ T cells. Nevertheless, T cell activation is associated with chromatin remodeling, albeit in a discrete and targeted way. CTCF has been previously implicated in playing a role in the establishment of TAD structures during embryonic cell development.[60] In line with this we have previously demonstrated that CTCF knockdown, a known regulator of genome organization, prevented terminal CD8$^+$ T cell differentiation by disrupting CTCF binding at weak-affinity binding sites. This served to promote a memory CD8$^+$ T cell transcriptional program at the expense of one more indicative of CD8$^+$ T cell effector differentiation.[42] A specific CTCF binding site at an effector-specific enhancer in the type I chemokine locus was also identified to insulate CCL3 expression, suggesting that CTCF may be important for regulation of specific enhancer-promoter interactions. Further, depletion of YY1, a protein known to regulate looping within CTCF-mediated chromatin loops,[61] also prevented the formation of terminal effector cells. Together these studies demonstrate that the chromatin architecture associated with CD8$^+$ T cell naive, effector, and memory states is orchestrated by differentiation-state-specific factors. The stepwise switch in chromatin organization associated with differentiation and the simultaneous loss of the naive T cell program, and engagement of a new set of factors including CTCF and YY1, induce appropriate chromatin reorganization necessary to sustain the differentiation of effector/memory CD8$^+$ T cells.

Limitations of the study

A limitation of HI-C, as with any technique that profiles populations of cells, is that the readout is an average of interactions occurring within the cells profiled. As such, Hi-C is unable to capture interactions that occur within sub-populations of the cells studied. In this study, owing to the rarity of virus-specific CD8$^+$ T cells at memory time points, we were unable to profile memory subsets independently, and as such, our data will likely reflect an averaged profile of central and effector memory T cells. Furthermore, the sequencing depth required to profile chromatin interactions at ultra-high resolution (low to sub-kilobase), and particularly for primary cells where interaction profiles are likely to exhibit heterogeneity between cells, is currently prohibitive. As such, interactions occurring across relatively short distances cannot be resolved (shorter than 100 kb in this study).

STAR★METHODS

Detailed methods are provided in the online version of this paper and include the following:

- KEY RESOURCES TABLE
- RESOURCE AVAILABILITY
  - Lead contact
  - Materials availability
  - Data and code availability
- EXPERIMENTAL MODEL AND STUDY PARTICIPANT DETAILS
  - Mice
  - Primary cell cultures
- METHOD DETAILS
  - ATAC-seq
  - ChIP and FAIRE
  - Hi-C

- Data normalization, differential loop calling, gene assignment, MDS plots, GSEA
- Data visualization
- Flow cytometry

- QUANTIFICATION AND STATISTICAL ANALYSIS

SUPPLEMENTAL INFORMATION

Supplemental information can be found online at https://doi.org/10.1016/j.celrep.2023.113301.

ACKNOWLEDGMENTS

We thank the Monash Flowcore facility (Monash University, Clayton) for helpful advice and technical assistance with flow cytometry and cell-sorting experiments and the Monash Micromon Genomics (Monash University, Clayton) and Hudson Genomics (Hudson Institute, Monash University Health and Medical Precinct, Clayton) facilities for advice relating to preparation and sequencing of Hi-C and ATAC-seq samples. Bioinformatic analyses were performed by the Monash Bioinformatics Platform, and mice were bred and housed at the Monash Animal Research Platform at Monash University, Clayton. Thanks to the Goldrath, Turner, and La Gruta laboratories for technical advice, helpful discussion, and critical reading of the manuscript. This work was supported by grants from the National Health and Medical Research Council of Australia, APP1003131 (S.J.T.); an Australian Research Council Discovery Grant, DP170102020 (S.J.T.); a joint Monash University-University of California, San Diego Seed Development grant (S.J.T. and A.W.G.); an NIH P01AI13212 (A.W.G.) and NIH grant AI102853 (C.M.).

AUTHOR CONTRIBUTIONS

Conceptualization, B.E.R., S.Q., B.Y., and S.J.T.; methodology, B.E.R., J.L., K.T., and P.D.; investigation, B.E.R., B.Y., J.L., J.K.C., S.N., A.E.M., V.A.U., T.J.B., I.A.P., and A.L.S.; software, K.T.; formal analysis, B.E.R., K.T., P.D., M.O., Z.H., P.F.H., A.B., M.S., and D.P.; resources, A.K.; writing - original draft, B.E.R.; writing - reviewing & editing, B.E.R., S.J.T., S.Q., A.W.G., P.C., C.M., and A.K.; supervision, S.J.T., A.W.G., D.P., C.M., and P.C.; funding acquisition, S.J.T. A.W.G., and C.M.

DECLARATION OF INTERESTS

A.W.G. is a member of the scientific advisory board of ArsenalBio. No funding from ArsenalBio was provided for this work.

INCLUSION AND DIVERSITY

We support inclusive, diverse, and equitable conduct of research.

Received: May 31, 2022
Revised: August 7, 2023
Accepted: October 3, 2023
Published: October 19, 2023

REFERENCES

1. Jenkins, M.R., Kedzierska, K., Doherty, P.C., and Turner, S.J. (2007). Heterogeneity of effector phenotype for acute phase and memory influenza A virus-specific CTL. J. Immunol. *179*, 64–70.
2. Crawford, A., Angelosanto, J.M., Nadwodny, K.L., Blackburn, S.D., and Wherry, E.J. (2011). A role for the chemokine RANTES in regulating CD8 T cell responses during chronic viral infection. PLoS Pathog. *7*, e1002098. https://doi.org/10.1371/journal.ppat.1002098.
3. Russ, B.E., Olshansky, M., Li, J., Nguyen, M.L.T., Gearing, L.J., Nguyen, T.H.O., Olson, M.R., McQuilton, H.A., Nüssing, S., Khoury, G., et al. (2017). Regulation of H3K4me3 at Transcriptional Enhancers Characterizes Acquisition of Virus-Specific CD8(+) T Cell-Lineage-Specific Function. Cell Rep. *21*, 3624–3636. https://doi.org/10.1016/j.celrep.2017.11.097.
4. La Gruta, N.L., Turner, S.J., and Doherty, P.C. (2004). Hierarchies in cytokine expression profiles for acute and resolving influenza virus-specific CD8+ T cell responses: correlation of cytokine profile and TCR avidity. J. Immunol. *172*, 5553–5560. https://doi.org/10.4049/jimmunol.172.9.5553.
5. Kaech, S.M., Hemby, S., Kersh, E., and Ahmed, R. (2002). Molecular and functional profiling of memory CD8 T cell differentiation. Cell *111*, 837–851. https://doi.org/10.1016/s0092-8674(02)01139-x.
6. Lalvani, A., Brookes, R., Hambleton, S., Britton, W.J., Hill, A.V., and McMichael, A.J. (1997). Rapid effector function in CD8+ memory T cells. J. Exp. Med. *186*, 859–865.
7. Veiga-Fernandes, H., Walter, U., Bourgeois, C., McLean, A., and Rocha, B. (2000). Response of naive and memory CD8+ T cells to antigen stimulation in vivo. Nat. Immunol. *1*, 47–53. https://doi.org/10.1038/76907.
8. Russ, B.E., Olshanksy, M., Smallwood, H.S., Li, J., Denton, A.E., Prier, J.E., Stock, A.T., Croom, H.A., Cullen, J.G., Nguyen, M.L.T., et al. (2014). Distinct Epigenetic Signatures Delineate Transcriptional Programs during Virus-Specific CD8(+) T Cell Differentiation. Immunity *41*, 853–865. https://doi.org/10.1016/j.immuni.2014.11.001.
9. Kouzarides, T. (2007). Chromatin modifications and their function. Cell *128*, 693–705, S0092-8674(07)00184-5 [pii]. https://doi.org/10.1016/j.cell.2007.02.005.
10. Johanson, T.M., Lun, A.T.L., Coughlan, H.D., Tan, T., Smyth, G.K., Nutt, S.L., and Allan, R.S. (2018). Transcription-factor-mediated supervision of global genome architecture maintains B cell identity. Nat. Immunol. *19*, 1257–1264. https://doi.org/10.1038/s41590-018-0234-8.
11. Scott-Browne, J.P., López-Moyado, I.F., Trifari, S., Wong, V., Chavez, L., Rao, A., and Pereira, R.M. (2016). Dynamic Changes in Chromatin Accessibility Occur in CD8+ T Cells Responding to Viral Infection. Immunity *45*, 1327–1340. https://doi.org/10.1016/j.immuni.2016.10.028.
12. Yu, B., Zhang, K., Milner, J.J., Toma, C., Chen, R., Scott-Browne, J.P., Pereira, R.M., Crotty, S., Chang, J.T., Pipkin, M.E., et al. (2017). Epigenetic landscapes reveal transcription factors that regulate CD8(+) T cell differentiation. Nat. Immunol. *18*, 573–582. https://doi.org/10.1038/ni.3706.
13. Zhang, J.A., Mortazavi, A., Williams, B.A., Wold, B.J., and Rothenberg, E.V. (2012). Dynamic transformations of genome-wide epigenetic marking and transcriptional control establish T cell identity. Cell *149*, 467–482. https://doi.org/10.1016/j.cell.2012.01.056.
14. Barski, A., Cuddapah, S., Cui, K., Roh, T.Y., Schones, D.E., Wang, Z., Wei, G., Chepelev, I., and Zhao, K. (2007). High-resolution profiling of histone methylations in the human genome. Cell *129*, 823–837. https://doi.org/10.1016/j.cell.2007.05.009.
15. Intlekofer, A.M., Takemoto, N., Wherry, E.J., Longworth, S.A., Northrup, J.T., Palanivel, V.R., Mullen, A.C., Gasink, C.R., Kaech, S.M., Miller, J.D., et al. (2005). Effector and memory CD8+ T cell fate coupled by T-bet and eomesodermin. Nat. Immunol. *6*, 1236–1244. https://doi.org/10.1038/ni1268.
16. Kallies, A., Xin, A., Belz, G.T., and Nutt, S.L. (2009). Blimp-1 transcription factor is required for the differentiation of effector CD8(+) T cells and memory responses. Immunity *31*, 283–295. https://doi.org/10.1016/j.immuni.2009.06.021.
17. Rutishauser, R.L., Martins, G.A., Kalachikov, S., Chandele, A., Parish, I.A., Meffre, E., Jacob, J., Calame, K., and Kaech, S.M. (2009). Transcriptional repressor Blimp-1 promotes CD8(+) T cell terminal differentiation and represses the acquisition of central memory T cell properties. Immunity *31*, 296–308. https://doi.org/10.1016/j.immuni.2009.05.014.
18. Man, K., Miasari, M., Shi, W., Xin, A., Henstridge, D.C., Preston, S., Pellegrini, M., Belz, G.T., Smyth, G.K., Febbraio, M.A., et al. (2013). The transcription factor IRF4 is essential for TCR affinity-mediated metabolic

programming and clonal expansion of T cells. Nat. Immunol. *14*, 1155–1165. https://doi.org/10.1038/ni.2710.

19. Danilo, M., Chennupati, V., Silva, J.G., Siegert, S., and Held, W. (2018). Suppression of Tcf1 by Inflammatory Cytokines Facilitates Effector CD8 T Cell Differentiation. Cell Rep. *22*, 2107–2117. https://doi.org/10.1016/j.celrep.2018.01.072.

20. Delpoux, A., Marcel, N., Hess Michelini, R., Katayama, C.D., Allison, K.A., Glass, C.K., Quiñones-Parra, S.M., Murre, C., Loh, L., Kedzierska, K., et al. (2021). FOXO1 constrains activation and regulates senescence in CD8 T cells. Cell Rep. *34*, 108674. https://doi.org/10.1016/j.celrep.2020.108674.

21. Kerdiles, Y.M., Beisner, D.R., Tinoco, R., Dejean, A.S., Castrillon, D.H., DePinho, R.A., and Hedrick, S.M. (2009). Foxo1 links homing and survival of naive T cells by regulating L-selectin, CCR7 and interleukin 7 receptor. Nat. Immunol. *10*, 176–184. https://doi.org/10.1038/ni.1689.

22. Roychoudhuri, R., Clever, D., Li, P., Wakabayashi, Y., Quinn, K.M., Klebanoff, C.A., Ji, Y., Sukumar, M., Eil, R.L., Yu, Z., et al. (2016). BACH2 regulates CD8(+) T cell differentiation by controlling access of AP-1 factors to enhancers. Nat. Immunol. *17*, 851–860. https://doi.org/10.1038/ni.3441.

23. Bulger, M., and Groudine, M. (2011). Functional and mechanistic diversity of distal transcription enhancers. Cell *144*, 327–339. https://doi.org/10.1016/j.cell.2011.01.024.

24. Heintzman, N.D., Stuart, R.K., Hon, G., Fu, Y., Ching, C.W., Hawkins, R.D., Barrera, L.O., Van Calcar, S., Qu, C., Ching, K.A., et al. (2007). Distinct and predictive chromatin signatures of transcriptional promoters and enhancers in the human genome. Nat. Genet. *39*, 311–318. https://doi.org/10.1038/ng1966.

25. Sekimata, M., Pérez-Melgosa, M., Miller, S.A., Weinmann, A.S., Sabo, P.J., Sandstrom, R., Dorschner, M.O., Stamatoyannopoulos, J.A., and Wilson, C.B. (2009). CCCTC-binding factor and the transcription factor T-bet orchestrate T helper 1 cell-specific structure and function at the interferon-gamma locus. Immunity *31*, 551–564. https://doi.org/10.1016/j.immuni.2009.08.021.

26. Li, P., Mitra, S., Spolski, R., Oh, J., Liao, W., Tang, Z., Mo, F., Li, X., West, E.E., Gromer, D., et al. (2017). STAT5-mediated chromatin interactions in superenhancers activate IL-2 highly inducible genes: Functional dissection of the Il2ra gene locus. Proc. Natl. Acad. Sci. USA. *114*, 12111–12119. https://doi.org/10.1073/pnas.1714019114.

27. Agarwal, S., and Rao, A. (1998). Modulation of chromatin structure regulates cytokine gene expression during T cell differentiation. Immunity *9*, 765–775. https://doi.org/10.1016/s1074-7613(00)80642-1.

28. Avni, O., Lee, D., Macian, F., Szabo, S.J., Glimcher, L.H., and Rao, A. (2002). T(H) cell differentiation is accompanied by dynamic changes in histone acetylation of cytokine genes. Nat. Immunol. *3*, 643–651. https://doi.org/10.1038/ni808.

29. Zheng, W., and Flavell, R.A. (1997). The transcription factor GATA-3 is necessary and sufficient for Th2 cytokine gene expression in CD4 T cells. Cell *89*, 587–596. https://doi.org/10.1016/s0092-8674(00)80240-8.

30. Shan, Q., Li, X., Chen, X., Zeng, Z., Zhu, S., Gai, K., Peng, W., and Xue, H.H. (2021). Tcf1 and Lef1 provide constant supervision to mature CD8(+) T cell identity and function by organizing genomic architecture. Nat. Commun. *12*, 5863. https://doi.org/10.1038/s41467-021-26159-1.

31. Araki, Y., Wang, Z., Zang, C., Wood, W.H., 3rd, Schones, D., Cui, K., Roh, T.Y., Lhotsky, B., Wersto, R.P., Peng, W., et al. (2009). Genome-wide analysis of histone methylation reveals chromatin state-based regulation of gene transcription and function of memory CD8+ T cells. Immunity *30*, 912–925. https://doi.org/10.1016/j.immuni.2009.05.006.

32. Sen, D.R., Kaminski, J., Barnitz, R.A., Kurachi, M., Gerdemann, U., Yates, K.B., Tsao, H.W., Godec, J., LaFleur, M.W., Brown, F.D., et al. (2016). The epigenetic landscape of T cell exhaustion. Science *354*, 1165–1169. https://doi.org/10.1126/science.aae0491.

33. Rao, S.S.P., Huntley, M.H., Durand, N.C., Stamenova, E.K., Bochkov, I.D., Robinson, J.T., Sanborn, A.L., Machol, I., Omer, A.D., Lander, E.S., and Aiden, E.L. (2014). A 3D map of the human genome at kilobase resolution reveals principles of chromatin looping. Cell *159*, 1665–1680. https://doi.org/10.1016/j.cell.2014.11.021.

34. Jenkins, M.R., Webby, R., Doherty, P.C., and Turner, S.J. (2006). Addition of a prominent epitope affects influenza A virus-specific CD8+ T cell immunodominance hierarchies when antigen is limiting. J. Immunol. *177*, 2917–2925. https://doi.org/10.4049/jimmunol.177.5.2917.

35. Battulin, N., Fishman, V.S., Mazur, A.M., Pomaznoy, M., Khabarova, A.A., Afonnikov, D.A., Prokhortchouk, E.B., and Serov, O.L. (2015). Comparison of the three-dimensional organization of sperm and fibroblast genomes using the Hi-C approach. Genome Biol. *16*, 77. https://doi.org/10.1186/s13059-015-0642-0.

36. Dixon, J.R., Jung, I., Selvaraj, S., Shen, Y., Antosiewicz-Bourget, J.E., Lee, A.Y., Ye, Z., Kim, A., Rajagopal, N., Xie, W., et al. (2015). Chromatin architecture reorganization during stem cell differentiation. Nature *518*, 331–336. https://doi.org/10.1038/nature14222.

37. Dixon, J.R., Selvaraj, S., Yue, F., Kim, A., Li, Y., Shen, Y., Hu, M., Liu, J.S., and Ren, B. (2012). Topological domains in mammalian genomes identified by analysis of chromatin interactions. Nature *485*, 376–380. https://doi.org/10.1038/nature11082.

38. Harmston, N., Ing-Simmons, E., Tan, G., Perry, M., Merkenschlager, M., and Lenhard, B. (2017). Topologically associating domains are ancient features that coincide with Metazoan clusters of extreme noncoding conservation. Nat. Commun. *8*, 441. https://doi.org/10.1038/s41467-017-00524-5.

39. Wang, W., Chandra, A., Goldman, N., Yoon, S., Ferrari, E.K., Nguyen, S.C., Joyce, E.F., and Vahedi, G. (2022). TCF-1 promotes chromatin interactions across topologically associating domains in T cell progenitors. Nat. Immunol. *23*, 1052–1062. https://doi.org/10.1038/s41590-022-01232-z.

40. Cresswell, K.G., Stansfield, J.C., and Dozmorov, M.G. (2020). SpectralTAD: an R package for defining a hierarchy of topologically associated domains using spectral clustering. BMC Bioinf. *21*, 319. https://doi.org/10.1186/s12859-020-03652-w.

41. Stansfield, J.C., Cresswell, K.G., and Dozmorov, M.G. (2019). multiHiCcompare: joint normalization and comparative analysis of complex Hi-C experiments. Bioinformatics *35*, 2916–2923. https://doi.org/10.1093/bioinformatics/btz048.

42. Quon, S., Yu, B., Russ, B.E., Tsyganov, K., Nguyen, H., Toma, C., Heeg, M., Hocker, J.D., Milner, J.J., Crotty, S., et al. (2023). DNA architectural protein CTCF facilitates subset-specific chromatin interactions to limit the formation of memory CD8(+) T cells. Immunity *56*, 959–978.e10. https://doi.org/10.1016/j.immuni.2023.03.017.

43. Zheng, R., Wan, C., Mei, S., Qin, Q., Wu, Q., Sun, H., Chen, C.H., Brown, M., Zhang, X., Meyer, C.A., and Liu, X.S. (2019). Cistrome Data Browser: expanded datasets and new tools for gene regulatory analysis. Nucleic Acids Res. *47*, D729–D735. https://doi.org/10.1093/nar/gky1094.

44. Chepelev, I., Wei, G., Wangsa, D., Tang, Q., and Zhao, K. (2012). Characterization of genome-wide enhancer-promoter interactions reveals co-expression of interacting genes and modes of higher order chromatin organization. Cell Res. *22*, 490–503. https://doi.org/10.1038/cr.2012.15.

45. Nüssing, S., Miosge, L.A., Lee, K., Olshansky, M., Barugahare, A., Roots, C.M., Sontani, Y., Day, E.B., Koutsakos, M., Kedzierska, K., et al. (2022). SATB1 ensures appropriate transcriptional programs within naive CD8(+) T cells. Immunol. Cell Biol. *100*, 636–652. https://doi.org/10.1111/imcb.12566.

46. Koay, H.F., Su, S., Amann-Zalcenstein, D., Daley, S.R., Comerford, I., Miosge, L., Whyte, C.E., Konstantinov, I.E., d'Udekem, Y., Baldwin, T., et al. (2019). A divergent transcriptional landscape underpins the development and functional branching of MAIT cells. Sci. Immunol. *4*, eaay6039. https://doi.org/10.1126/sciimmunol.aay6039.

47. Lieberman-Aiden, E., van Berkum, N.L., Williams, L., Imakaev, M., Ragoczy, T., Telling, A., Amit, I., Lajoie, B.R., Sabo, P.J., Dorschner, M.O.,

et al. (2009). Comprehensive mapping of long-range interactions reveals folding principles of the human genome. Science *326*, 289–293. https://doi.org/10.1126/science.1181369.

48. Denton, A.E., Russ, B.E., Doherty, P.C., Rao, S., and Turner, S.J. (2011). Differentiation-dependent functional and epigenetic landscapes for cytokine genes in virus-specific CD8+ T cells. Proc. Natl. Acad. Sci. USA. *108*, 15306–15311. https://doi.org/10.1073/pnas.1112520108.
49. Zediak, V.P., Johnnidis, J.B., Wherry, E.J., and Berger, S.L. (2011). Cutting edge: persistently open chromatin at effector gene loci in resting memory CD8+ T cells independent of transcriptional status. J. Immunol. *186*, 2705–2709, jimmunol.1003741 [pii]. https://doi.org/10.4049/jimmunol.1003741.
50. Northrop, J.K., Wells, A.D., and Shen, H. (2008). Cutting edge: chromatin remodeling as a molecular basis for the enhanced functionality of memory CD8 T cells. J. Immunol. *181*, 865–868. 181/2/865 [pii].
51. Shan, Q., Hu, S.S., Zhu, S., Chen, X., Badovinac, V.P., Peng, W., Zang, C., and Xue, H.H. (2022). Tcf1 preprograms the mobilization of glycolysis in central memory CD8(+) T cells during recall responses. Nat. Immunol. *23*, 386–398. https://doi.org/10.1038/s41590-022-01131-3.
52. Onrust-van Schoonhoven, A., de Bruijn, M.J.W., Stikker, B., Brouwer, R.W.W., Braunstahl, G.J., van IJcken, W.F.J., Graf, T., Huylebroeck, D., Hendriks, R.W., Stik, G., and Stadhouders, R. (2023). 3D chromatin reprogramming primes human memory T(H)2 cells for rapid recall and pathogenic dysfunction. Sci. Immunol. *8*, eadg3917. https://doi.org/10.1126/sciimmunol.adg3917.
53. Mortazavi, A., Williams, B.A., McCue, K., Schaeffer, L., and Wold, B. (2008). Mapping and quantifying mammalian transcriptomes by RNA-Seq. Nat. Methods *5*, 621–628. https://doi.org/10.1038/nmeth.1226.
54. Schmitt, S., Prestel, M., and Paro, R. (2005). Intergenic transcription through a polycomb group response element counteracts silencing. Genes Dev. *19*, 697–708. https://doi.org/10.1101/gad.326205.
55. Melé, M., and Rinn, J.L. (2016). Cat's Cradling" the 3D Genome by the Act of LncRNA Transcription. Mol. Cell *62*, 657–664. https://doi.org/10.1016/j.molcel.2016.05.011.
56. Isoda, T., Moore, A.J., He, Z., Chandra, V., Aida, M., Denholtz, M., Piet van Hamburg, J., Fisch, K.M., Chang, A.N., Fahl, S.P., et al. (2017). Non-coding Transcription Instructs Chromatin Folding and Compartmentalization to Dictate Enhancer-Promoter Communication and T Cell Fate. Cell *171*, 103–119.e18. https://doi.org/10.1016/j.cell.2017.09.001.
57. Utzschneider, D.T., Gabriel, S.S., Chisanga, D., Gloury, R., Gubser, P.M., Vasanthakumar, A., Shi, W., and Kallies, A. (2020). Early precursor T cells establish and propagate T cell exhaustion in chronic infection. Nat. Immunol. *21*, 1256–1266. https://doi.org/10.1038/s41590-020-0760-z.
58. Cai, S., Lee, C.C., and Kohwi-Shigematsu, T. (2006). SATB1 packages densely looped, transcriptionally active chromatin for coordinated expression of cytokine genes. Nat. Genet. *38*, 1278–1288. https://doi.org/10.1038/ng1913.
59. Danecek, P., Bonfield, J.K., Liddle, J., Marshall, J., Ohan, V., Pollard, M.O., Whitwham, A., Keane, T., McCarthy, S.A., Davies, R.M., and Li, H. (2021). Twelve years of SAMtools and BCFtools. GigaScience *10*, giab008. https://doi.org/10.1093/gigascience/giab008.
60. Chen, X., Ke, Y., Wu, K., Zhao, H., Sun, Y., Gao, L., Liu, Z., Zhang, J., Tao, W., Hou, Z., et al. (2019). Key role for CTCF in establishing chromatin structure in human embryos. Nature *576*, 306–310. https://doi.org/10.1038/s41586-019-1812-0.
61. Beagan, J.A., Duong, M.T., Titus, K.R., Zhou, L., Cao, Z., Ma, J., Lachanski, C.V., Gillis, D.R., and Phillips-Cremins, J.E. (2017). YY1 and CTCF orchestrate a 3D chromatin looping switch during early neural lineage commitment. Genome Res. *27*, 1139–1152. https://doi.org/10.1101/gr.215160.116.
62. Sidwell, T., Liao, Y., Garnham, A.L., Vasanthakumar, A., Gloury, R., Blume, J., Teh, P.P., Chisanga, D., Thelemann, C., de Labastida Rivera, F., et al. (2020). Attenuation of TCR-induced transcription by Bach2 controls regulatory T cell differentiation and homeostasis. Nat. Commun. *11*, 252. https://doi.org/10.1038/s41467-019-14112-2.
63. Buenrostro, J.D., Giresi, P.G., Zaba, L.C., Chang, H.Y., and Greenleaf, W.J. (2013). Transposition of native chromatin for fast and sensitive epigenomic profiling of open chromatin, DNA-binding proteins and nucleosome position. Nat. Methods *10*, 1213–1218. https://doi.org/10.1038/nmeth.2688.
64. Ramírez, F., Dündar, F., Diehl, S., Grüning, B.A., and Manke, T. (2014). deepTools: a flexible platform for exploring deep-sequencing data. Nucleic Acids Res. *42*, W187–W191. https://doi.org/10.1093/nar/gku365.
65. Rognes, T., Flouri, T., Nichols, B., Quince, C., and Mahé, F. (2016). VSEARCH: a versatile open source tool for metagenomics. PeerJ *4*, e2584. https://doi.org/10.7717/peerj.2584.
66. Li, H. (2013). Aligning sequence reads, clone sequences and assembly contigs with BWA-MEM. arXiv, 1303.3997. https://doi.org/10.48550/arXiv.1303.3997.
67. Servant, N., Lajoie, B.R., Nora, E.P., Giorgetti, L., Chen, C.J., Heard, E., Dekker, J., and Barillot, E. (2012). HiTC: exploration of high-throughput 'C' experiments. Bioinformatics *28*, 2843–2844. https://doi.org/10.1093/bioinformatics/bts521.
68. Durand, N.C., Shamim, M.S., Machol, I., Rao, S.S.P., Huntley, M.H., Lander, E.S., and Aiden, E.L. (2016). Juicer Provides a One-Click System for Analyzing Loop-Resolution Hi-C Experiments. Cell Syst. *3*, 95–98. https://doi.org/10.1016/j.cels.2016.07.002.
69. Robinson, M.D., McCarthy, D.J., and Smyth, G.K. (2010). edgeR: a Bioconductor package for differential expression analysis of digital gene expression data. Bioinformatics *26*, 139–140. https://doi.org/10.1093/bioinformatics/btp616.
70. Yu, Y., Ouyang, Y., and Yao, W. (2018). shinyCircos: an R/Shiny application for interactive creation of Circos plot. Bioinformatics *34*, 1229–1231. https://doi.org/10.1093/bioinformatics/btx763.
71. Ramírez, F., Ryan, D.P., Grüning, B., Bhardwaj, V., Kilpert, F., Richter, A.S., Heyne, S., Dündar, F., and Manke, T. (2016). deepTools2: a next generation web server for deep-sequencing data analysis. Nucleic Acids Res. *44*, W160–W165. https://doi.org/10.1093/nar/gkw257.
72. Wickham, H. (2016). ggplot2: Elegant Graphics for Data Analysis (Springer-Verlag).
73. Subramanian, A., Tamayo, P., Mootha, V.K., Mukherjee, S., Ebert, B.L., Gillette, M.A., Paulovich, A., Pomeroy, S.L., Golub, T.R., Lander, E.S., and Mesirov, J.P. (2005). Gene set enrichment analysis: a knowledge-based approach for interpreting genome-wide expression profiles. Proc. Natl. Acad. Sci. USA. *102*, 15545–15550. https://doi.org/10.1073/pnas.0506580102.

STAR★METHODS

KEY RESOURCES TABLE

REAGENT or RESOURCE	SOURCE	IDENTIFIER
Antibodies		
anti-CD45.1 (A20)	BD Biosciences	RRID:AB_395044
anti-CD8 (53–6.7)	BD Biosciences	RRID:AB_469400
anti-CD44 (IM7)	Biolegend	RRID:AB_830785
anti-CCL4	Thermo Fisher Scientific	RRID:AB_2551861
anti-CCL5	Biolegend	RRID:AB_2860706
Secondary Ab for CCL4	Thermo Fisher Scientific	RRID:AB_2534142
Bacterial and virus strains		
A/HKx31-OVA Influenza virus	Doherty Lab	Ref. [34]
Chemicals, peptides, and recombinant proteins		
Recombinant human IL-2	RnD Systems	N/A
Ovalubumin 257-264 peptide (SIINFEKL)	Auspep	N/A
Critical commercial assays		
Fixation/Permeabilisation Solution Kit	BD Biosciences	Cat# 555028
NEBNext CHIP-seq Library Prep Master Mix Set for Illumina	New England BioLabs	Cat# NEB #E6240L
Deposited data		
HiC and ATAC-Seq data	This manuscript	Accession GSE225885
Experimental models: Organisms/strains		
OT-I Transgenic mouse strain	Jackson Laboratories	RRID:IMSR_JAX:003831
C57BL/6J	Monash Animal Research Platform	RRID:IMSR_JAX:000664
Ccl5 Δ-5	This manuscript	
Ccl5 Δ-20	This manuscript	
Satb1$^{m1ANU/m1ANU}$	Turner Laboratory	Ref. [46]
Bach2fl/fl x CD4CRE	Provided by Prof Axel Kallies, The Peter Doherty Institute for Infection and Immunity	Ref. [62]
Software and algorithms		
Cistrome Toolkit	http://cistrome.org/	RRID:SCR_005396
Bedtools	https://github.com/arq5x/bedtools2	RRID:SCR_006646
SAMTOOLS	https://github.com/samtools/samtools	RRID:SCR_002105
HiTC	https://www.bioconductor.org/packages/release/bioc/html/HiTC.html	RRID:SCR_013175
ggplot2	https://github.com/tidyverse/ggplot2	RRID:SCR_014601
MACS2	https://github.com/macs3-project/MACS	RRID:SCR_013291
R	https://www.r-project.org/	RRID:SCR_001905
deepTools	https://github.com/deeptools/deepTools	RRID:SCR_016366
FlowJo v10	FlowJo	RRID:SCR_008520
MulitHiCcompare	https://bioconductor.org/packages/HiCcompare/	RRID:SCR_022368
Tidyverse	https://github.com/tidyverse	RRID:SCR_019186
Juicer	https://github.com/tidyverse	RRID:SCR_017226
BWA-MEM	https://github.com/lh3/bwa	RRID:SCR_022192
ShinyCircoss	https://github.com/YaoLab-Bioinfo/shinyCircos	RRID:SCR_022367

RESOURCE AVAILABILITY

Lead contact

Further information and requests for resources and reagents should be directed to and will be fulfilled by the lead contact, Prof Stephen Turner (stephen.j.turner@monash.edu).

Materials availability

CCL5 mouse lines are available contingent on signing of appropriate Material Transfer Agreements between Institutions. All other materials are freely available.

Data and code availability

Deposited HiC and ATAC-seq data from naive, effector, and memory $CD8^+$ OT-I T cells after influenza A virus infection; HiC data from naive $CD8^+$ $BACH2^{-/-}$ and naive $CD8^+$ $SATB1^{mAnu1/mAnu1}$ T cells (accession number GEO: GSE225885). All original code is publicly available as of the date of publication. RRIDs are listed in the Key resources table. Any additional information required to reanalyze the data reported in this paper is available from the lead contact upon request.

EXPERIMENTAL MODEL AND STUDY PARTICIPANT DETAILS

Mice

$Ly5.2^+$ C57BL/6J, *Satb1*$^{m1Anu/m1Anu}$, and $Ly5.1^+$ OT-I mice were bred and housed under specific-pathogen-free conditions at the Monash Animal Research Platform, with housing and experimental procedures approved by the Monash University Animal Ethics Committee. *Bach2*$^{fl/fl}$ x *Cd4Cre* mice were bred and housed under specific-pathogen-free conditions at the Department of Microbiology and Immunology Animal Facility at the University of Melbourne. All mice used were female, and aged 8–12 weeks old. For infection, mice were anesthetized and infected i.n. with 10^4 p.f.u. of recombinant A/HKx31 virus engineered to express the $OVA_{257–264}$ peptide (x31-OVA) in the neuraminidase stalk. For adoptive transfer studies, $CD45.1^+$ OT-I T cells were adoptively transferred into female $CD45.2^+$ recipients.

Primary cell cultures

Naive $CD8\alpha$+ CD44lo/int cells were sort-purified from C57BL/6J or Δ−5 kb and Δ−20 kb mice (8–12 weeks) (>99% purity). Cultures were initiated by stimulating 3.3 × 105 T cells with plate-bound anti-CD3ε (10μg/mL), anti-CD28 (5 μg/mL), and anti-CD11a (10μg/mL) antibodies, and cultured in the presence of IL-2 (10U/mL). Cells were cultured in 3mL RPMI, supplemented with 10% FCS (v/v), 2mM L-glutamine, and penicillin and streptomycin in 6-well plates, before being expanded into T25 flasks (10mls media) after 72hrs, T75 flasks at 96hrs (20mL media). Cultures were harvested at 120hrs.

METHOD DETAILS

ATAC-seq

We used an ATAC-seq protocol adapted from.[63] Nuclei were extracted from 50,000 naive, effector or memory, sort-purified OT-1 cells and immediately resuspended in transposition reaction mix (Illumina Nextera DNA Sample Preparation Kit - Cat #FC121-1030) for 30 min at 37C. Transposed DNA was purified using a QIAGEN MinElute PCR Purification kit (Cat #28004), and amplified for 5 PCR cycles using PCR primer 1 (Ad1_noMX) and an indexed PCR primer. Aliquots of each amplicon were used as template in a real-time quantitative PCR for 20 cycles to determine the optimal cycle number for library amplification, with amplicons purified as previously. Library quality was determined using a Bioanalyzer (Agilent) to ensure that amplicons ranged between 50 and 200bp, and samples were subjected to paired-end sequencing on an Illumina Hiseq2500 instrument. Sequence data were mapped to UCSC mm10, then filtered for PCR duplicates and blacklisted regions, then shifted using Alignment Sieve (deepTools;[64]) and lastly peaks were called with MACS2 (https://github.com/macs3-project/MACS).

ChIP and FAIRE

Effector T cells were crosslinked with 0.6% formaldehyde for 10 min at RT. Following sonication, immune-precipitation was performed with anti-H3K4me3, H3K27me3 or HK3K27Ac ChIP-grade antibodies and Protein A magnetic beads (Millipore). FAIRE was performed on samples fixed and sonicated as per ChIP, with accessible chromatin extracted twice with phenol:chloroform:i-soamyl (25:24:1) (Sigma). FAIRE enrichment was normalized against a total input for which reverse cross-linking had been performed. ChIP and FAIRE enrichment was measured using quantitative real-time PCR, with data normalized against a total input and no-antibody control. Primers used in these assays were reported previously.[3]

Hi-C

Hi-C was performed as per Rao,[33] with the following adjustments: Step 2 - cells were fixed with 1.5% formaldehyde for 10 min at RT. Step 7 - the nuclei extraction buffer contained 0.4% Igepal. Step 12 - restriction digestion was performed overnight with 400U Mbo1

(NEB) in NEB buffer 2.1. Steps 28–35 were skipped. Step 54 - 2.5 μl NEBNext Adapter for Illumina (cat #E7370) was used in place of Illumina indexed adapter, with ligation at 20C for 15 min, followed by addition of 3U USER enzyme and further incubation at 37C for 15min. Step 60 - samples were incubated at 95C for 10 min in a thermocycler, and beads were removed before final library amplification with NEBNext Multiplex Oligos for Illumina (cat #E7335S).

Data normalization, differential loop calling, gene assignment, MDS plots, GSEA

Fastq files were pre-processed into single end reads in a custom workflow with VSEARCH[65] to overlap or blunt end join R1 and R1, and SeqKit (https://github.com/shenwei356/seqkit) to remove PCR duplicates. Processed fastq reads were then mapped to the mouse reference, mm10 with BWA-MEM[66] with the following flags, (-M, -K 10000000, -5) and converted into bam files with SAMtools.[59] Intragenic contacts were extracted with a custom C script that generated a three column table (region1, region2, chromsome_name) which could be quantized into any bin sizes. Depending on the downstream analysis different bin sizes were used: 50 kb for differential looping and TADs, 1 Mb for A/B calling. An R script using the 'data.table' package (https://github.com/Rdatatable/data.table) was used to quantize the raw contacts table into a binned table with the following columns (chromosome_name, region1, region2, IF), where IF is interaction frequency. A/B compartments were called using the HiTC R package,[67] TADs were called with SpectralTAD,[40] Hi-C data were normalized and differential loops were called using multiHiCcompare[41] including cyclic loess joint normalization and differential loops calling. Binned Hi-C matrices generated using Juicer.[68]

GSEA analysis was performed using the FGSEA package (https://www.biorxiv.org/content/10.1101/060012v3), with bubble plots made using a custom Tidyverse script (https://www.tidyverse.org/). MDS plots were generated using the edgeR MDS function.[69] Positioning of dots in MDS is directly proportional to sample similarity. For gene assignments, loop ends were annotated with a gene using in house script, where genes were assigned to either end of the loop if the overlap was no more than 25kb from the end of the loop.

Domain changes were identified by performing pairwise correlation of Hi-C interaction frequencies at 50kb resolution. Where the correlation was inverse, we defined that as a domain change between the samples being compared. Where contiguous regions of inverse correlation were identified, the regions were merged and counted as a single domain change.

Data visualization

Circos plots were generated using the ShinyCircos package.[70] Enrichment plots were made using the deepTools2 package.[71] All other figures were made using custom R codes and ggplots2.[72]

Flow cytometry

Single-cell suspensions from spleens, lymph nodes or bronchiolar lavage fluid (BAL) were stained with LIVE/DEAD Fixable Aqua Dead Cell Stain (Thermo Fischer Scientific) for 10 min at room temperature. Cells were washed with MACS buffer (2mM EDTA, 2% BSA in PBS) prior to resuspension in antibody cocktail containing fluorochrome conjugated antibodies specific for CD4, CD8α, CD45.1, or CD44. For cytokine staining, cells were fix and permeabilized according to manufacturer's instructions (BD Biosciences) prior to staining with anti-CCL4 and CCL5 antibodies. Stained cells were washed twice with permeabilization buffer, and twice with MACS buffer before analysis. Samples were read with a FACSCanto II cytometers (BD Biosciences), and analyzed using FlowJo software (Tree Star, Ashland, OR, USA).

QUANTIFICATION AND STATISTICAL ANALYSIS

In Figure 2, RNA-seq data are shown as the mean of 2 (memory) or 3 (naive and effector) biological replicate values, ±SEM. In Figure 3A, numbers of *cis* interactions unique to each differentiation state were determined by pairwise comparisons using multiHiCcompare (50 kb resolution, 0.05 FDR). 3B) GSEA analysis comparing genes connected by loops enriched in one condition over another (Y axis), against RNA-seq data derived from matching samples.[8] Circle sizes reflect adjusted p values (-log10) and color represents normalized enrichment score (NES), with red indicating enrichment versus the first RNA-seq condition listed in pairwise comparison, and blue indicating enrichment is the second RNA-seq condition listed. In Figure 4 enrichment of transcription factor binding at enhancers unique to naive or effector[3] was performed using curated transcription factor ChIP-Seq data through the CistromeDB Toolkit with shading reflecting GIGGLE score.[43] In Figures 5 and 6, GSEA analysis comparing genes connected by loops gained in naive Bach2$^{-/-}$ and *Satb1*$^{m1Anu/m1Anu}$ CD8^{+} T cells, respectively, relative to naive WT CD8^{+} T cells against RNA-seq data derived from naive and effector CTLs samples (datasets as described above). p values and normalized enrichment score (NES) are shown.[73] All other Methods used to quantify and perform statistical analyses on data are described in figure legends.